Scilight

Regenerative Medicine and Dentistry
https://www.sciltp.com/journals/rmd

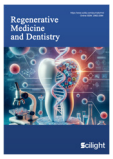

Article

Photo-Curable GelMA-Chitosan Bioadhesive Hydrogel: An Evaluation of Mechanical and Adhesive Properties

Sattwikesh Paul [1,2,3,*], Karsten Schrobback [4], Phong Anh Tran [1,3], Christoph Meinert [1,3,5], Angus Weekes [1,3], Jordan William Davern [1,3,6] and Travis Jacob Klein [1,3,6,*]

[1] Centre for Biomedical Technologies, Queensland University of Technology, 60 Musk Ave., Kelvin Grove, QLD 4059, Australia
[2] Department of Surgery and Radiology, Gazipur Agricultural University (GAU), Gazipur 1706, Bangladesh
[3] School of Mechanical, Medical and Process Engineering, Queensland University of Technology (QUT), 2 George Street, Brisbane, QLD 4000, Australia
[4] School of Biomedical Sciences, Centre for Genomics and Personalised Health, Translational Research Institute, Queensland University of Technology (QUT), 37 Kent Street, Woolloongabba, QLD 4102, Australia
[5] Gelomics Pty Ltd., Brisbane, QLD 4059, Australia
[6] ARC Training Centre for Cell and Tissue Engineering Technologies, Queensland University of Technology (QUT), Brisbane, QLD 4059, Australia
* Correspondence: paulsattwik@gmail.com or paulsattwik@gau.edu.bd or sattwikesh.paul@hdr.qut.edu.au (S.P.); t2.klein@qut.edu.au (T.J.K.)

How To Cite: Paul, S.; Schrobback, K.; Tran, P.A.; et al. Photo-Curable GelMA-Chitosan Bioadhesive Hydrogel: An Evaluation of Mechanical and Adhesive Properties. *Regenerative Medicine and Dentistry* **2025**, *2*(3), 15. https://doi.org/10.53941/rmd.2025.100015

Received: 21 August 2025
Revised: 15 September 2025
Accepted: 26 September 2025
Published: 28 September 2025

Abstract: Polymer-based adhesives are used in tissue repair; however, their application is frequently limited by suboptimal mechanical or adhesive properties. This study aims to develop a natural polymer-based photo-cross-linkable and structurally robust bioadhesive hydrogel, utilizing gelatin methacryloyl (GelMA) and chitosan. We compared the mechanical properties and adhesiveness of various GelMA-chitosan hydrogel formulations cross-linked by three different photo-initiator systems—[tris (2,2′-bipyridyl) dichlororuthenium (II) hexahydrate ([RuII (bpy)3]$^{2+}$ and sodium persulfate (Ru/SPS), lithium acylphosphinate (LAP), and 1-[4-(2-hydroxyethoxy)-phenyl]-2-hydroxy-2-methyl-1-propanone (Irgacure 2959)]. The Ru/SPS cross-linked GelMA-chitosan hydrogel showed a higher compressive modulus than GelMA hydrogel at both neutral and alkaline pHs, suggesting potential use during infection or delayed wound healing. Chitosan addition to GelMA significantly enhanced hydrogel adhesiveness, with Ru/SPS cross-linked hydrogel exhibiting the highest adhesive strength to cartilage (tensile: ~100 kPa) and skin (tensile: ~25 kPa, lap shear: ~43 kPa). Rheological analysis confirmed the shear-thinning behaviour of the hydrogel precursor solution, indicating its injectability. Moreover, the hydrogel demonstrated robust adhesion to cartilage and skin during ex vivo joint movement and skin bend tests, suggesting its utility in dynamic tissue environments. This study suggests that Ru/SPS cross-linked GelMA-chitosan hydrogel is a promising natural polymer-based bioadhesive, warranting further exploration in a variety of tissue repair applications.

Keywords: hydrogel; bioadhesive; cartilage; skin; photo-initiators; GelMA; chitosan; photo-cross-linking

1. Introduction

Tissue repair applications often require filling or covering an irregular injured area with a biomaterial. In such applications, the biomaterial must fit the defect and integrate with surrounding tissues to remain in place, provide mechanical support, and improve healing. While, traditionally, biomaterials have been fixed to surrounding tissues

using sutures, an emerging alternative solution to these challenges is to use bioadhesive hydrogels [1]. Hydrogels are three-dimensional structures of cross-linked hydrophilic polymers extensively used in regenerative medicine and wound healing. Hydrogels, with their high water absorption capacity and adaptable structural properties [2,3] provide a suitable microenvironment similar to extracellular matrix (ECM) [3–5], facilitating cell migration, adhesion, proliferation, and differentiation while delivering nutrients and growth factors [3–5]. The properties of hydrogels can be modified to mimic the physicochemical and biological characteristics required for specific tissue architectures through chemical functionalization and physical manipulation [6,7]. Bioadhesive hydrogels are currently employed in numerous biomedical applications, including scaffolds in tissue engineering [1], mucosal adhesives to prolong drug release at specific sites [8], and substitutes for sutures to minimize the risk of infection [9].

While synthetic polymers can create durable hydrogels, they frequently lack bio-functionalities, including adhesion motifs and biodegradation sites [10]. Such constraints typically necessitate the addition of bioactive compounds [11], or the utilization of natural polymers. Natural polysaccharide-based hydrogels have demonstrated the ability to guide cell migration and proliferation in tissue regeneration [12–14], and do not produce toxic degradation products [15]. Chitosan, a polycationic deacetylated derivative of chitin, has been explored extensively for developing bioadhesives and hydrogels in regenerative medicine [16–19], because it is biocompatible, biodegradable, antibacterial and mucoadhesive [20–23]. The amino groups in chitosan facilitate ionic complexes with anionic polymers or chemical functionalization with various cross-linkable groups [24–27]. Chitosan is utilized for cartilage repair [28–32], wound healing [33], and medical dressings [34,35]. While chitosan and its derivatives form brittle hydrogels [36], blending with other natural polymers can improve their mechanical characteristics [37,38]. Gelatin methacryloyl (GelMA) is an ideal choice for this purpose, due to its photo-cross-linking capabilities, adjustable mechanical properties, and biocompatibility [39]. GelMA can cross-link under moderate conditions, enabling cell encapsulation [40], and has been utilized in wound adhesive and lung sealant formulations [41,42]. GelMA has limitations in terms of its mechanical properties and degradation rate, which hinder its suitability for designing load-bearing tissues [43,44]. However, its mechanical properties can be tailored by altering the concentration [45,46], cross-linking time [46], degree of methacrylation [45,47], and copolymerization with other components [40].

Photo-cross-linking, or light-based cross-linking, provides precise control over the mechanical properties of hydrogels [48,49]. The benefits of photo-cross-linking compared to conventional physical or chemical cross-linking methods include the precise control of the polymerization process, rapid cross-linking, and negligible heat generation [50]. Visible light-sensitive photo-initiators enable the cross-linking of photosensitive hydrogels using visible light, thus avoiding the potential side effects of UV light, such as DNA damage and cell death [51]. In this context, several photo-initiators have been extensively studied [52], such as lithium with type II photo-initiators utilizing ruthenium (Ru) and sodium persulfate (SPS) of interest [53–55] due to their diverse cross-linking mechanisms.

Following this rationale, in this study, we combined chitosan with GelMA to develop a natural polymer-based bioadhesive hydrogel, utilizing visible light photo-initiators Ru/SPS for potential applications in various tissue repair and regenerative medicine contexts. Since both chitosan and GelMA form mechanically weak hydrogels on their own, we initially hypothesized that combining chitosan with GelMA will enhance the mechanical properties of hydrogel. To examine this, we evaluated the mechanical characteristics of GelMA-chitosan hydrogels at varying concentrations cross-linked by three different photo-initiators utilizing our previously established protocol [53]. Chitosan is soluble in acidic pH, therefore we investigated the influence of pH on the mechanical properties of GelMA-chitosan hydrogels. Furthermore, we postulated that the inherent adhesive potential of chitosan and the addition of Ru/SPS cross-linking would improve the adhesive characteristics of GelMA-chitosan hydrogels. We evaluated the bioadhesive characteristics of the GelMA-chitosan hydrogel by conducting qualitative and quantitative tests on animal tissues, specifically cartilage and skin. We assessed the injectability of GelMA-chitosan hydrogel precursor solution by examining its rheological properties and tested its applicability in ex vivo investigations using hypodermic needles.

2. Experimental

2.1. Hydrogels Synthesis

GelMA stock solution (35%; *w*/*v*) was prepared by dissolving sterile lyophilized GelMA polymer (gelatin methacryloyl, porcine skin, type A, 80% DoF, Lot No. LU20L03, Gelomics Pty Ltd., Brisbane, Australia) in phosphate buffered saline (PBS) (Thermo Fisher, Waltham, MA, USA). Chitosan (75–85% deacetylated, Sigma-Aldrich, St. Louis, MO, USA, Cat. No. 448877) was autoclaved as a suspension in Milli-Q water at 121 °C for 15 min and subsequently dissolved by adding a filter-sterilized previously prepared solution of 1% (*v*/*v*) acetic acid and 150 mm sodium chloride (NaCl) (Sigma-Aldrich, USA) and stirring at room temperature (RT) for 48 h to

make 3% (*w*/*v*) stock solution [38]. GelMA-chitosan blends were prepared by combining GelMA (10%, 15%, and 20% *w*/*v*) with chitosan (0.5% or 1% *w*/*v*). The mixture was shaken at 37 °C for 5 min at 750 RPM using a thermoshaker (Eppendorf AG 22331 Hamburg, Germany), and then vortexed (Maxi Mix II Vortex Mixer, Thermo Scientific, USA) for 45 s and stored at 4 °C overnight.

Photo-initiator stock solutions [50 mM Ru (tris (2,2′-bipyridyl) dichlororuthenium (II) hexahydrate ($[RuII(bpy)_3]^{2+}$), 1M SPS (sodium persulfate); 3% (*w*/*v*) LAP (lithium phenyl-2, 4, 6-trimethylbenzoylphosphinate) (all Sigma-Aldrich, USA); and 3% (*w*/*v*) Irgacure (IC2959, 1-[4-(2-hydroxyethoxy)-phenyl]-2-hydroxy-2-methyl-1-propanone; BASF, Ludwigshafen, Germany)] were freshly made in PBS and 0.22 μm filter sterilized on the day of hydrogel construct preparation.

Hydrogel constructs were prepared as described elsewhere [56]. Briefly, GelMA-chitosan solutions were mixed with either 0.5 mM Ru/20 mM SPS, 0.15% (*w*/*v*) LAP or 0.25% (*w*/*v*) Irgacure at 37 °C. Precursor solutions were then transferred into a Teflon casting mould, covered with a glass slide [both sterilized with 70% (*v*/*v*) ethanol] and cross-linked either in a LED cross-linker (Luna Crosslinker, Gelomics, Australia) for 5 min (Ru/SPS) or 3 min (LAP) at 405 nm or a UV cross-linker (CL-1000 crosslinker, UVP, Upland, CA, USA) for 15 min (Irgacure) at 365 nm. For compression test, hydrogel constructs were cut to dimension (length × width × height: 4 mm × 4 mm × 2 mm) with a scalpel and acrylic hydrogel cutting guides. The adhesion test involved injecting hydrogel precursor solution into the application site using a 1 or 5 mL syringe with a 19-gauge hypodermic needle. GelMA hydrogels without chitosan were considered as the control in each group.

2.2. Mechanical Properties

2.2.1. Compression Testing

The compressive modulus (CM) of GelMA and GelMA-chitosan hydrogels was determined by uniaxial unconfined compression testing [56]. Briefly, the weight of freshly prepared hydrogels was taken before and after overnight incubation at 37 °C. The hydrogels were incubated for 24 h with PBS solution (pH: 7.4), while in the pH study, all hydrogels were incubated for 2 h with pH adjusted PBS solutions (pH 5, 6, 7, 8 and 9). Hydrogel samples were imaged with a stereomicroscope (Stereoscope_NikonBoomStand, Nikon SMZ745T, Japan), and the cross-sectional area was determined by Image J software (National Instruments, USA). A compression test was conducted using an Instron 5567 (Instron, Norwood, Massachusetts, USA) with a nonporous indenter and a 5 or 500 N-load cell at 37 °C using a custom-made immersion bath with PBS (pH: 7.4) [56] or PBS with adjusted pH (pH 5, 6, 7, 8 and 9) in the pH study. The displacement rate was set at 0.01 mm/s until > 15% compressive strain was reached. The height of each hydrogel was determined from the force-displacement curve as the point at which force started to deviate significantly from zero [56]. The CM was calculated by analyzing the slope of the stress-strain curve in a strain range of 10 to 15%.

2.2.2. Swelling Ratio (SR)

The determination of the equilibrium swelling of hydrogels was conducted according to previously established methods [46]. Briefly, freshly prepared hydrogels were weighed before (W_{before}) and after (W_{after}) incubation at 37 °C for 24 h with PBS (pH: 7.4). In the pH study, hydrogels were incubated for 2 h in different pH adjusted PBS solutions (pH 5, 6, 7, 8 and 9). The equilibrium swelling ratio was quantified as a percentage and determined using the following method:

$$\text{Swelling ratio (SR)} = \{(W_{after} - W_{before})/W_{before}\} \times 100\%$$

2.2.3. GelMA-Chitosan Polymer Interactions at Different pH (pH Study)

Interactions between GelMA and chitosan polymers at different pH levels were assessed using a pH-based mechanical and SR analysis of GelMA and GelMA-chitosan hydrogels. GelMA and GelMA-chitosan hydrogels were synthesized according to the protocols described in the hydrogel synthesis section. The hydrogels were then incubated at 37 °C with pH adjusted different PBS solutions (pH 5, 6, 7, 8 and 9) for two hours. The samples were weighed before and after the incubation [(extra PBS was blotted by Kim-wipes (Kimtech Science, Mississauga, ON, USA) before weighing], and the SR was calculated as described in the SR determination section. The compression test was carried out as described in the compression testing section employing pH-adjusted PBS solutions (pH 5, 6, 7, 8 and 9) in the immersion bath for each group.

2.3. Adhesive Properties

2.3.1. Osteochondral Construct Preparation

The adhesive strength of GelMA and GelMA-chitosan hydrogels in a joint setting was assessed using osteochondral constructs, and the adhesion test was carried out in accordance with the previously published protocol of our group [53]. Briefly, fresh bovine stifle joints (1–3 years of age) were purchased from a butcher shop. The joint was kept moist during transport to the laboratory (one hour) and all explant procedures by regular rinsing with PBS supplemented with 100 U/mL of penicillin and 100 µg/mL of streptomycin (both from Invitrogen®, Waltham, MA, USA). For further processing, the joint capsule and surrounding tissues were removed, and the osteochondral constructs (height: 15–20 mm, diameter: 5 mm) were harvested from the femoral condyles by a trephine. The superficial layer of cartilage was removed with a sterile scalpel. Two osteochondral constructs were then placed into a medical-grade silicone tube (length: 10 mm, inner diameter: 5 mm, wall thickness: 0.6 mm; Gecko Optical, Perth, WA, Australia), with the cartilage surfaces facing each other. For all samples, a space of around 1 mm was maintained between two constructs. Freshly prepared hydrogel precursor solution was injected into the void space between two osteochondral constructs using a 1 mL syringe fitted with a 19-gauge needle. The cross-linking process was carried out using either an LED cross-linker for 5 min (Ru/SPS) or 3 min (LAP) at a wavelength of 405 nm, or a UV cross-linker for 15 min (Irgacure) at a wavelength of 365 nm. After cross-linking, the constructs were incubated at 37 °C with PBS (pH: 7.4) for one hour.

2.3.2. Adhesive Strength Determination

The adhesive strength of the hydrogel was assessed by performing a uniaxial tensile test using an Instron 5567 machine fitted with a 500 N load cell. The osteochondral constructs supported by a silicone tube were transferred to the Instron and securely held in place using a custom-made acrylic grip. The silicone tube was removed prior to the test with a scalpel. The displacement rate was set at 0.01 mm/sec, and tensile modulus (TM) was determined at 0–3% strain. The stereomicroscopic images of osteochondral constructs taken before and after the test were used to ascertain the actual gap between two osteochondral constructs and the point of hydrogel failure using Image J software (National Instruments, Austin, TX, USA). In each of the groups and conditions, a total of four (n = 4) osteochondral constructs were utilized.

2.3.3. Length Measurement of Adherent Hydrogels from Nearest Issue

To quantitatively assess the adhesive or cohesive failure of hydrogels in the osteochondral constructs following the adhesion test, the length (mm) of the hydrogels adhering to the nearest cartilage tissue was measured using stereomicroscopic images and analysed using Image J software (version 1.53c) (National Instruments, USA). The length of hydrogel in osteochondral constructs was determined by measuring three specific points in the stereomicroscopic images. The point of osteochondral construct without adherent hydrogel was considered as 0 mm.

2.3.4. Ex Vivo Joint Durability Test

The durability of in situ cross-linked GelMA and GelMA-chitosan hydrogel in a joint environment was evaluated using an ex vivo model in accordance with the previously published protocol of our group [53]. Briefly, a bovine stifle joint (collected from a butcher shop) was clamped in the sample preparation table to replicate joint alignment, and the joint capsule was incised to provide a clean view of the femoral condyles. A biopsy punch was used to produce circular chondral defects (diameter: 8 mm, area: 0.5 cm^2) in the condyles by excising cartilage down to the subchondral bone (defect depth: ~2 mm). GelMA and GelMA-chitosan hydrogel precursor solutions containing Ru/SPS or LAP were injected into the defects using a 5 mL syringe equipped with a 19-gauge needle. A specially designed stand was utilized to place an LED light source (LIGHTFE Keychain Blacklight, UV 395 nm UV light LED source, China) above the defective area, with a fluorinated ethylene propylene film (DuPont™ Teflon® FEP film, USA) affixed to prevent the spillover of hydrogel precursor solution and to aid in the process of photo-cross-linking by ensuring the light penetration [53]. After photo-cross-linking, the joint was flexed and extended approximately thirty times to simulate joint movement in a fluid-free condition, as described in our previous study [53].

The adhesiveness of GelMA and GelMA-chitosan hydrogels cross-linked with Ru/SPS and LAP, with or without chitosan, to cartilage was compared through a joint movement investigation utilizing Indian ink (Parker Quink, France) staining. Briefly, after cross-linking the hydrogel into the chondral defects (diameter: 10 mm, area: 0.8 cm^2), the surface was painted with blue Indian ink (20%; *v*/*v* in PBS) for 15 s and excess stain was removed

using a moist cotton swab. The Indian ink will leave a permanent mark on the uneven hydrogel surface and in locations where the integration of the hydrogel is disrupted. The presence of Indian ink at the hydrogel-cartilage interface was determined by analysing the photographs of the stained hydrogel-cartilage interface before and after the joint movement test using the Image J software. The hydrogels were attempted to be detached from the defect site by applying repeated (5 times) fingertip pressure.

2.4. Skin Adhesion

2.4.1. In Vitro Wound Closure Test

The wound closure strengths of the hydrogels were assessed using the standard test technique for wound closure strength of tissue adhesives and sealants, ASTM F2458–05 [57], with specific adjustments. Briefly, fresh caprine skin was procured from a nearby abattoir and the adipose tissue layer was removed. After shaving the superficial layer with a razor blade, skin samples (thickness: 2.5 mm) were cut into rectangular pieces (length × wide: 20 mm × 10 mm) and stored in PBS (pH: 7.4) at room temperature for 10 min before the experiments. To prepare the samples, the skin was blotted with Kimwipe to remove the excess liquid. Two skin samples were adhered (adhesive area: 20 mm × 8 mm) to acrylic pieces (Supplementary Figure S1A) using Super glue (Selleys®, Fix&Go™ Super Glue, Australia), leaving a 20 mm × 2 mm area free from the acrylic. The acrylic-mounted skin samples were placed on a prefabricated mounting plate with a support structure designed to maintain a 3 mm gap between the two skin samples (Figure 1A). Approximately 150 µL of the Ru/SPS containing GelMA or GelMA-chitosan hydrogel precursor solution was injected into the gap (length × wide × thickness: 20 mm × 3 mm × 2.5 mm) between two skin samples. The samples and support structure were subsequently transferred to a cross-linker box (Luna Crosslinker, Gelomics, Australia) and cross-linked with visible light (405 nm) at room temperature for 5 min. Following cross-linking, the acrylic pieces and support structure were transferred to an Instron 68TM-30 electromechanical testing device (Instron 68TM-30, Illinois Tool Works Inc. (ITW), Norwood, MA, USA) equipped with a 100 N load cell. Before starting the test, the support structure was removed and the sample was stretched at the constant rate of 50 mm/min. The TM was determined at 0–3% strain and the adhesive strength was calculated as the maximum load divided by the adhesive contact area (length × width).

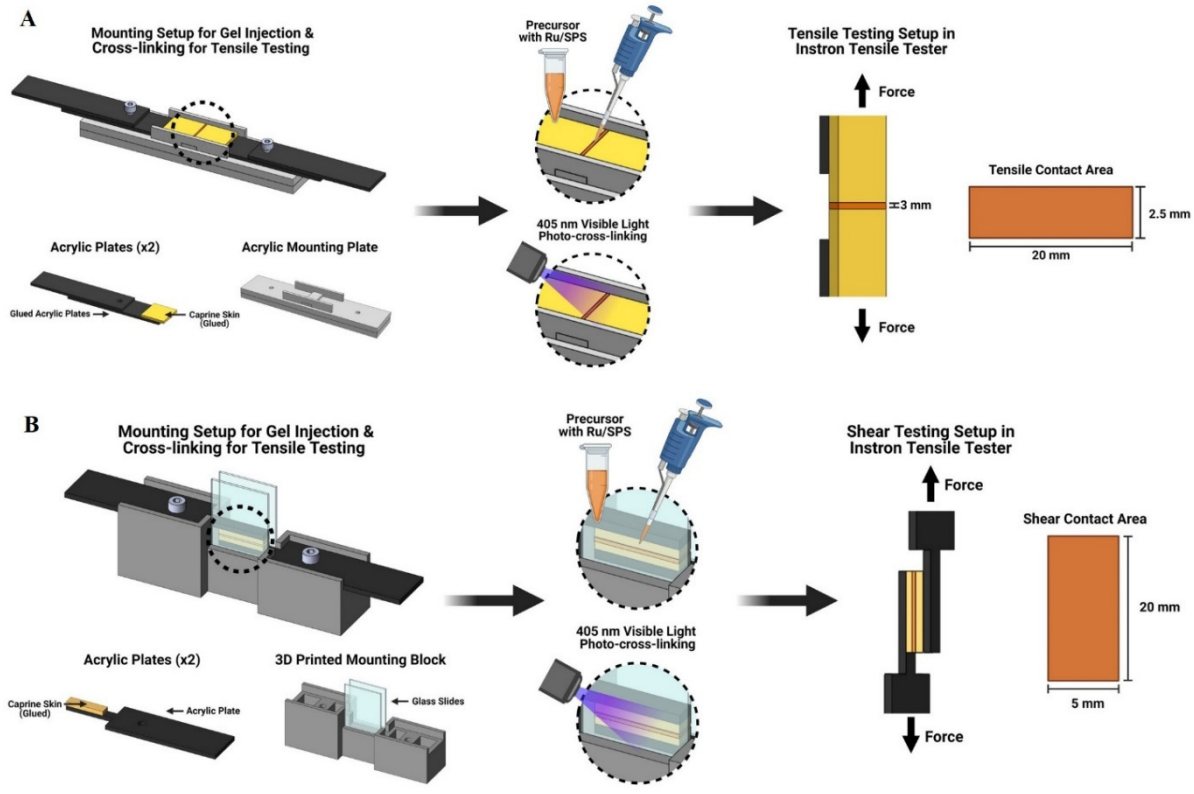

Figure 1. Skin sample preparation and adhesion test. Schematic representation of (**A**) tensile adhesion test and (**B**) lap shear test of caprine skin on Instron 68TM-30 with 100 N load cell. Figure created with BioRender.com.

2.4.2. Skin Bend Test

Bioadhesive hydrogels, particularly those applied to functional tissues like skin, must maintain strong adhesion under dynamic physiological movements like walking, running or other routine activities for effectiveness. To evaluate the adhesive properties of Ru/SPS cross-linked GelMA and GelMA-chitosan hydrogel under simulated skin movement, a skin bend test was performed following a tensile test using caprine skin. Briefly, after the tensile test, one end of the skin sample, adhered to the hydrogel, was bent multiple times. Subsequently, the hydrogel was assessed for the existence of cracks, deformities, or detachment, both during and after the test.

2.4.3. In Vitro Lap Shear Test

The shear strength of the Ru/SPS cross-linked GelMA and GelMA-chitosan hydrogel was evaluated based on the standardised testing methodology ASTM F2255-05 [58]. Briefly, fresh caprine skin was procured from a nearby abattoir and the adipose tissue layer was removed. Skin samples were shaved and cut into rectangular pieces (thickness: 2.5 mm; length × wide: 20 mm × 5 mm), stored in PBS (pH: 7.4) for 10 min before the test at room temperature. Two samples were adhered to prefabricated acrylic sheets using Super glue and positioned in a custom-made mould with overlapping condition, leaving a 1 mm gap between them (Figure 1B). Approximately 100 µL of hydrogel precursor solution was injected into the gap using a 19-gauge needle attached to a 1 mL syringe. Subsequently, the mould containing the sample was transferred to a visible light cross-linker (Luna Crosslinker, Gelomics, Australia) and cross-linked at 405 nm for 5 min at room temperature. The construct was then placed in an Instron 68TM-30 electromechanical testing device (Instron 68TM-30, USA) equipped with a 100 N load cell. Prior to commencing the test, the support mould was removed, and the sample was subjected to a consistent stretching rate of 5 mm/min. The shear modulus (SM) was measured within the range of 0–3% strain, while the shear strength (SS) was computed by dividing the highest load by the adhesive contact area (length × width).

2.5. Rheology of Hydrogel Precursor Solution

2.5.1. Rheology Sample Preparation

Rheometry was performed on Ru/SPS containing GelMA, chitosan and GelMA-chitosan solutions. The samples were kept in a thermo-shaker (Eppendorf AG 22331 Hamburg, Germany) at 37 °C before conducting the rheological characterization. The photo-initiators were mixed with the hydrogel solution and kept protected from light. The mixing process was carried out by pipetting up and down at 37 °C, followed by a brief centrifugation (20 s) (Tomy microOne, Japan) to eliminate any bubbles.

2.5.2. Rheological Characterization

The rheological characteristics of hydrogel precursor solutions were examined using a compact rheometer (MCR 302, Anton Paar, Germany) that had a Peltier plate for controlling the temperature. The investigation on shear rheology was performed using a cone plate (CP25-1) with a 25 mm diameter, a one-degree angle, and a fixed gap of 0.05 mm. All rheological studies were conducted at a constant temperature of 37 °C, with no solvent trap utilized because earlier verification proved that the samples did not dry during testing. The sample (230 µL per sample; n = 3) was transferred to the rheometer plate. Following the positioning of plate and trimming of the samples, all investigations commenced after a 2-min stabilization phase to ensure mechanical and thermal equilibrium. The measurements were conducted using a HETD400 hood with the airflow deactivated to prevent desiccation and ensure a consistent sample temperature. Shear rate sweeps ranging from 0.01 to 1000 1/s were performed to observe the phenomenon of shear thinning and measure the viscosity.

In addition, oscillatory strain, frequency, and temperature sweeps were conducted using a conventional 24 mm parallel plate geometry with a 0.15 mm gap. Strain sweeps (0.01–100%) were used to observe the linear viscoelastic (LVE) regions of hydrogel precursor solutions at a constant frequency of 1 Hz. The oscillatory frequency sweeps were performed within the LVE range (1% strain and frequency of 0.1–100 Hz) to monitor the dynamic rheological behaviour. Finally, temperature sweep experiments were performed from 40–4 °C with a 1 °C/min decrease ramp to determine the gel point. The storage modulus (G′) and loss modulus (G″) were measured at a constant frequency of oscillation (f = 1 Hz) and strain (γ = 1%), and the gelation point was estimated based on the crossover of G′ and G″ values.

2.5.3. Statistical Analysis

Analysis of all data was performed in GraphPad Prism (version 9; Graph-Pad, Boston, MA, USA). The sample sizes for the compression and cartilage adhesion tests were 6 and 4 hydrogels in each group, respectively. For the tensile and lap shear tests conducted on skin tissue, the sample sizes were 8 and 10, respectively for each group. Quantitative data on mechanical and adhesive properties are analysed using two-way ANOVA with Tukey's multiple comparisons tests. Statistically significant differences were considered at $p < 0.05$ for all tests and are indicated in figures using asterisks.

3. Results

3.1. Addition of Chitosan to GelMA Increases Compressive Modulus and Decreases Swelling Ratio

Chitosan [36] and chitosan hydrogels [37] have poor mechanical properties, but combining it with other polymers can overcome this shortcoming and improve the overall mechanical properties of the hydrogel [37,56,59]. In this study, chitosan significantly increased CM of hydrogels across all photo-initiator groups (Figures 2A, S2 and S3A,C). GelMA-chitosan (GelMA 15% and chitosan 1%, *w*/*v*) hydrogels cross-linked by Ru/SPS, LAP and Irgacure revealed higher CM (245.7 ± 6.1 kPa, 235.9 ± 7.0 kPa and 272.9 ± 13.4 kPa, respectively) compared to GelMA (15%, *w*/*v*) hydrogels (164.5 ± 4.9 kPa, 179.3 ± 8.4 kPa and 165.4 ± 2.9 kPa, respectively) in their specific groups. A similar phenomenon was observed in all photo-initiators groups with 10% (*w*/*v*) and 20% (*w*/*v*) GelMA. Significant differences in CM of 15% (*w*/*v*) GelMA hydrogels containing 1% and 0.5% (*w*/*v*) chitosan were observed in all photo-initiators groups, with 1% (*w*/*v*) chitosan hydrogels showing higher CM than others. Hydrogels containing 15% (*w*/*v*) GelMA and 0.5% (*w*/*v*) chitosan cross-linked by Ru/SPS and LAP showed a comparable CM to GelMA hydrogels in their respective groups; however, this difference was highly significant in the Irgacure group (Figure 2A).

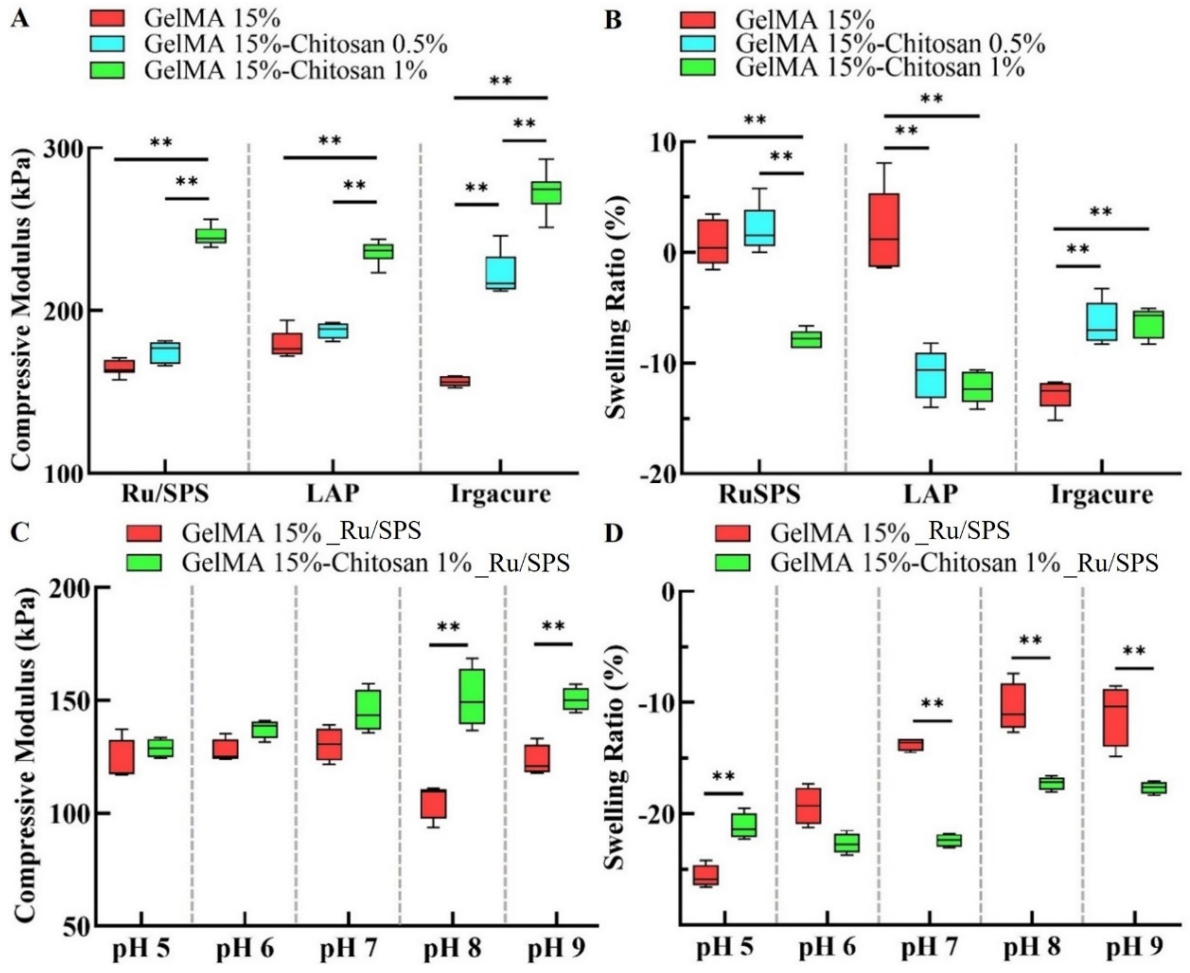

Figure 2. Compressive modulus and swelling ratio of GelMA and GelMA-chitosan hydrogels. 15% (*w*/*v*) GelMA alone or blended with 0.5% and 1% (*w*/*v*) chitosan hydrogels were cross-linked with Ru/SPS, LAP and Irgacure photo-initiators. (**A**) compressive modulus of hydrogels was measured 24 h after polymerization using an Instron

5567 tester with a nonporous indenter and a 5 N load cell. (**B**) The swelling ratio was determined by weighing hydrogels directly after polymerization and after 24 h of incubation in PBS (pH = 7.4). (**C**,**D**) 15% (*w*/*v*) GelMA alone or blended with 1% (*w*/*v*) chitosan hydrogels were cross-linked with Ru/SPS and incubated in pH-adjusted PBS. (**C**) Compressive modulus of hydrogels was measured 2 h after polymerization using an Instron 5567 tester with a nonporous indenter and a 500 N load cell. (**D**) The swelling ratio was determined by weighing hydrogels directly after polymerization and after 2 h of incubation in pH adjusted PBS. Significant differences are indicated by asterisks ** ($p < 0.01$) between groups (n = 6 (**A**,**B**) or 4 (**C**,**D**) for each group).

The SR provides preliminary indication of the mechanical properties and offers valuable insight into in vivo applicability of hydrogels. Excessive swelling can compromise the mechanical characteristics of hydrogels, causing additional stress on adjacent tissues or resulting in hydrogel extrusion after application. The addition of chitosan (1%, *w*/*v*) to GelMA (15%, *w*/*v*) hydrogels cross-linked with Ru/SPS and LAP reduced their SR, while the opposite effect was observed for Irgacure cross-linked hydrogels (Figures 2B and S3B,D).

Considering the disparities in charge between chitosan and GelMA, we anticipated ionic interactions between them and hence hypothesized that the pH levels might influence the mechanical properties of GelMA-chitosan hydrogels. The study examined the impact of pH on the mechanical properties of Ru/SPS cross-linked GelMA (GelMA 15%, *w*/*v*) and GelMA-chitosan (GelMA 15% and chitosan 1%, *w*/*v*) hydrogels by measuring their CM and SR in pH-adjusted PBS solutions (pH 5, 6, 7, 8 and 9). In this study, the pH significantly influenced the relative CM of hydrogels at pH 8 and 9, with GelMA-chitosan hydrogels exhibiting a higher CM compared to GelMA hydrogels. However, no significant differences of CM were observed at other pH levels (Figure 2C). This study found pH-dependent swelling in all hydrogels (Figure 2D). GelMA hydrogels revealed an increase in SR as pH increased (range −28% to −10%). GelMA-chitosan hydrogels showed a higher SR than GelMA hydrogels at pH 5, but a more negative SR at pH 7, 8, and 9 (Figure 2D).

3.2. Addition of Chitosan Increases GelMA Hydrogel Adhesive Properties

The adhesive properties of bioadhesives are determined by the cohesive strength of the material and the adhesive strength between the material and the adherent tissue [16,60]. In this study, chitosan had a substantial effect on the tensile modulus (TM), ultimate tensile strength (UTS), tensile strain at maximum load (TSML), and toughness of hydrogels. The addition of 1% (*w*/*v*) chitosan with 15% (*w*/*v*) GelMA exhibited a significant increase of TM of GelMA-chitosan hydrogels compared to GelMA hydrogels cross-linked by Irgacure (Figure 3A). Although Ru/SPS cross-linked GelMA-chitosan hydrogels (GelMA 15% and chitosan 1%, *w*/*v*) represented a comparable TM (162.5 ± 10.0 kPa) to 15% (*w*/*v*) GelMA hydrogels (157.3 ± 31.5 kPa), the values were high relative to other cross-linking systems (Figure 3A). A similar trend was observed in GelMA-chitosan hydrogels with 10% and 20% (*w*/*v*) GelMA cross-linked by Ru/SPS (Supplementary Figure S4A,E). Chitosan (1%, *w*/*v*) significantly increased hydrogel UTS with 15% and 20% (*w*/*v*) GelMA in the Ru/SPS group, compared to controls (Figures 3B and S4F). A similar phenomenon was observed in 10% and 15% (*w*/*v*) GelMA containing 1% (*w*/*v*) chitosan hydrogels cross-linked by LAP and Irgacure, respectively (Figures 3B and S4B). Ru/SPS cross-linked GelMA-chitosan (GelMA 15% and chitosan 1%, *w*/*v*) hydrogels exhibited an increased TSML (0.6 ± 0.1 mm/mm) compared to 15% (*w*/*v*) GelMA hydrogels (Figure 3C). Moreover, chitosan (1%, *w*/*v*) significantly increased hydrogel toughness with 15% and 20% (*w*/*v*) GelMA in the Ru/SPS group compared to controls (Figures 3D and S4H).

GelMA-chitosan (GelMA 15% and chitosan 1%, *w*/*v*) hydrogels showed hydrogel failure in the hydrogel itself (cohesive failure); however, most failures in the GelMA (15%, *w*/*v*) hydrogels occurred from the hydrogel-cartilage interface (adhesive failure) (Figures 3E,F and S5A,B,D). The addition of 1% (*w*/*v*) chitosan to 10% and 15% (*w*/*v*) GelMA significantly increased adherent hydrogel length (0.44 ± 0.1 mm and 0.31 ± 0.1 mm), respectively, over GelMA controls (0 ± 0 mm and 0.03 ± 0.1 mm), respectively, in the Ru/SPS group (Figures 3F and S5A). A similar trend was observed in 10% and 20% (*w*/*v*) GelMA containing 1% (*w*/*v*) chitosan hydrogels cross-linked by Irgacure (Supplementary Figure S5A,B). However, the difference was non-significant in the LAP group irrespective of the concentrations of GelMA and chitosan used (Figures 3F and S5A,B).

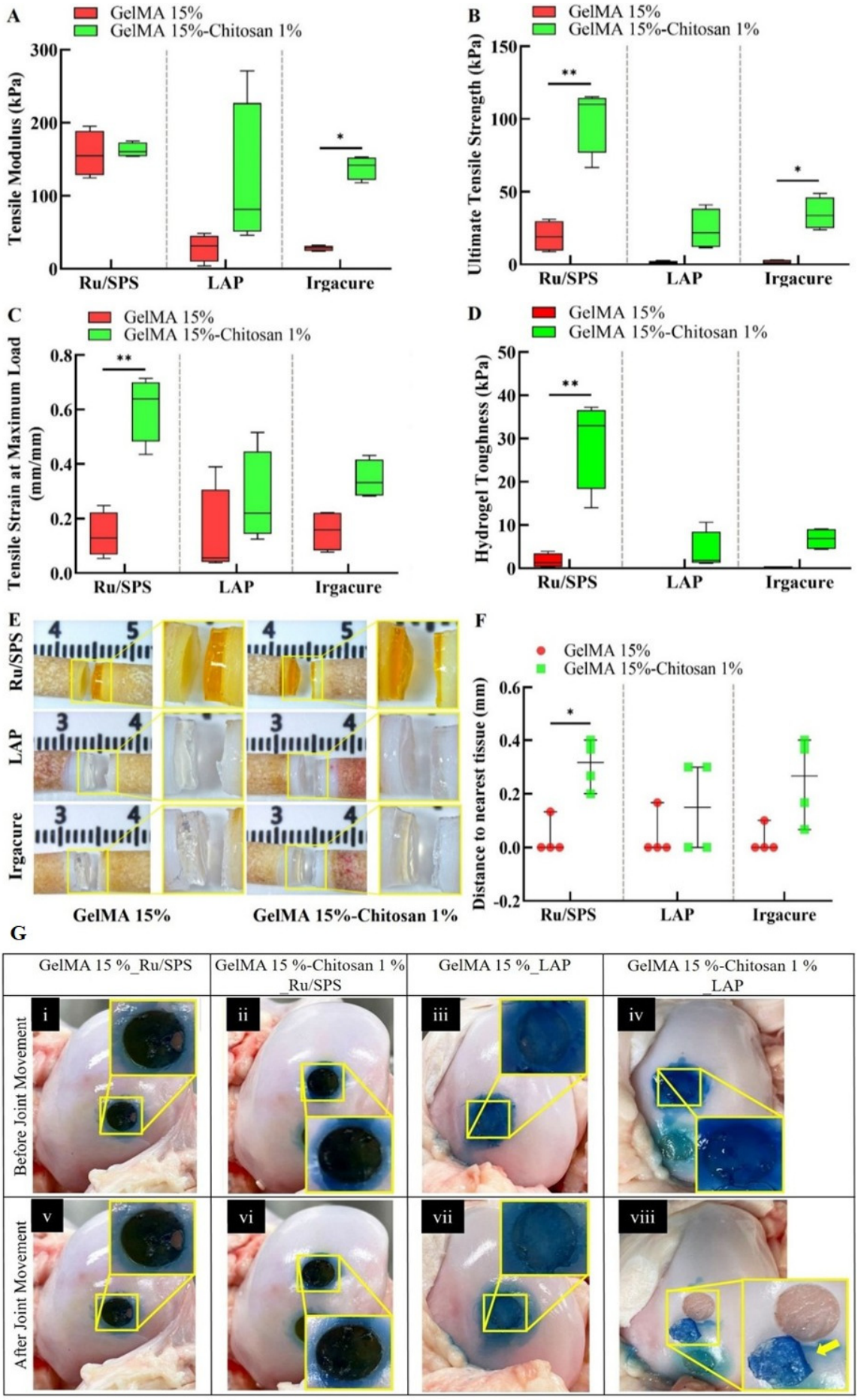

Figure 3. Effects of chitosan on cartilage adhesive properties of GelMA and GelMA-chitosan hydrogels. 15% (*w*/*v*) GelMA alone or blended with 1% (*w*/*v*) chitosan hydrogels were cross-linked with Ru/SPS, LAP and Irgacure

photo-initiators in between the cartilage surfaces of bovine osteochondral cores. (**A**) Tensile modulus, (**B**) ultimate tensile strength, (**C**) tensile strength at maximum load and (**D**) hydrogel toughness were measured after polymerization and after 1 h incubation with PBS (pH = 7.4). (**E**) Images of the osteochondral cores and hydrogels after adhesion tests; area of interest is marked in the inset. (**F**) Length of hydrogel to nearest cartilage tissue was measured after adhesion tests (0 mm indicates no hydrogel on the tissue). Significant differences are indicated by asterisks * ($p < 0.05$) and ** ($p < 0.01$) between groups (n = 4 for each group). (**G**) Ex vivo adhesion test of in situ cross-linked hydrogels in bovine joint. Integration of 15% (*w*/*v*) GelMA alone or blended with 1% (*w*/*v*) chitosan hydrogels with Ru/SPS or LAP photo-initiator in full-thickness cartilage defects (8 mm diameter) in bovine knee joints, before (**i**–**iv**) and after (**v**–**viii**) joint movement study; dislodged hydrogels are marked with a yellow arrow. Hydrogels were stained with Indian Ink for visualization purposes.

3.3. Ru/SPS Cross-Linked GelMA-Chitosan Hydrogels Are Resilient in Cartilage Defects of Bovine Joints Ex Vivo

A bovine ex vivo joint study was conducted to evaluate the durability of GelMA-chitosan (GelMA 15% and chitosan 1%, *w*/*v*) hydrogels under joint conditions[37]. In this study, the Ru/SPS cross-linked GelMA hydrogels with or without chitosan (1%, *w*/*v*) demonstrated uniform surface morphology and remarkable adhesion to cartilage defects (Figure 3G(v,vi)). The LAP cross-linked 15% (*w*/*v*) GelMA hydrogel was able to retain the hydrogel-cartilage integration; however, the chitosan-containing hydrogel was dislodged from the defect site during the joint movement study (Figure 3G(vii,viii)).

3.4. Adding Chitosan to GelMA Hydrogel Enhances Its Adhesive Properties to Skin Tissue

The adhesive properties of Ru/SPS cross-linked GelMA (15%, *w*/*v*) and GelMA-chitosan (GelMA 15% and chitosan 1%, *w*/*v*) hydrogels were assessed through a uniaxial tensile test on fresh caprine skin (n: 8 each group) (Supplementary Video S1 and S2), based on promising mechanical and adhesion test results of these polymer-PI combinations with bovine cartilage. Although the addition of 1% (*w*/*v*) chitosan to 15% (*w*/*v*) GelMA did not result in a significant increase of TM of GelMA-chitosan (81.0 ± 10.8 kPa) hydrogels compared to GelMA (76.6 ± 9.5 kPa) hydrogels alone in caprine skin, it did lead to a notable enhancement in UTS (24.7 ± 6.2 kPa) compared to the GelMA hydrogel group (15.8 ± 2.4 kPa) (Figure 4A,B). Similar phenomena were observed in TSML and tensile toughness, where GelMA-chitosan hydrogel exhibited significantly higher values (0.3 ± 0.1 kPa) and (4.3 ± 2.1 kPa) compared to GelMA hydrogels (0.2 ± 0.0 kPa) and (1.9 ± 0.3 kPa), respectively (Figure 4C,D).

In the skin bend test (n = 3 for each group), two of three GelMA hydrogel samples broke apart, resulting in separation at the break site, indicating insufficient mechanical strength and adhesion to sustain tissue movement (Figure 4I(vii,viii), Supplementary Video S3–S5). However, the GelMA-chitosan hydrogel exhibited stronger adhesion to the skin across all samples (n = 3) (Figure 4I(x–xii), Supplementary Video S6–S8), indicating more robust mechanical and adhesive properties compared to GelMA hydrogel, suggesting its potential suitability for dynamic environments where tissue movement is a factor.

In lap shear tests (n = 10 each group), the incorporation of chitosan (1%, *w*/*v*) into GelMA (15%, *w*/*v*) hydrogels did not result in a statistically significant change in the shear modulus (SM), ultimate shear strength (USS), shear strength at maximum load (SSML) or shear toughness (Figure 4E–H). However, both of the hydrogels showed promising adhesive properties when utilizing Ru/SPS cross-linking system (Supplementary Video S9 and S10). Notably, the shear strength observed in this study is higher than that of other hydrogels studied elsewhere for skin wound healing applications [61–65].

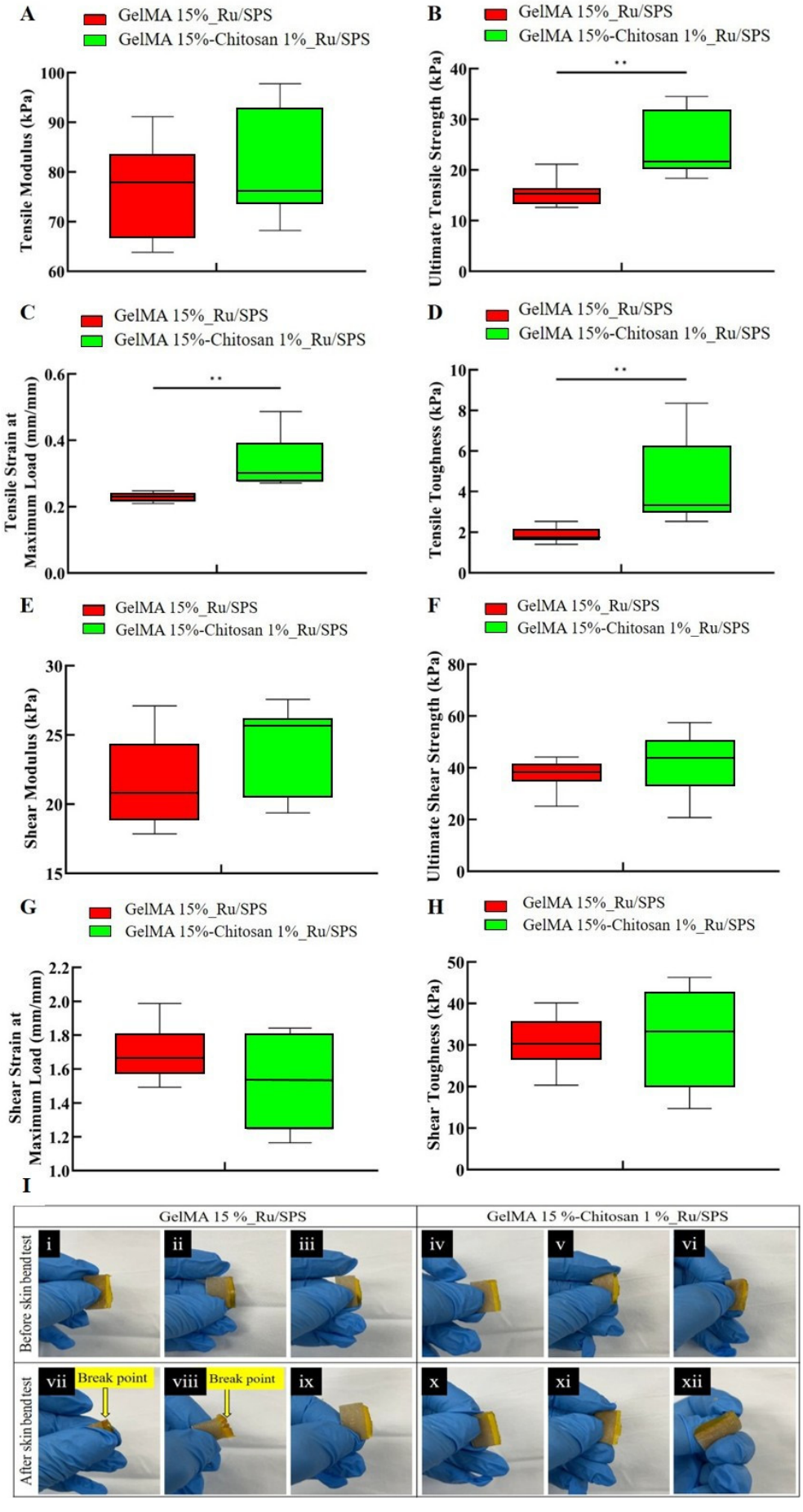

Figure 4. Effects of chitosan on the skin adhesive properties of GelMA and GelMA-chitosan hydrogels. 15% (*w*/*v*) GelMA alone or blended with 1% (*w*/*v*) chitosan hydrogels were cross-linked with Ru/SPS in caprine skin. (**A**)

Tensile modulus, (**B**) ultimate tensile strength, (**C**) tensile strength at maximum load and (**D**) tensile toughness (**E**) shear modulus, (**F**) ultimate shear strength, (**G**) shear strength at maximum load and (**H**) shear toughness were measured after polymerization at room temperature (sample size tensile test, n: 8; shear test, n = 10). GelMA group was used as a control for each group. Significant differences are indicated by asterisks * ($p < 0.05$) and ** ($p < 0.01$) between groups. (**I**) Ex vivo adhesion test of in situ cross-linked hydrogels in caprine skin. Adhesion of Ru/SPS cross-linked 15% (*w*/*v*) GelMA alone or blended with 1% (*w*/*v*) chitosan hydrogels to caprine skin (20 mm × 2.5 mm contact area) before (**i**–**vi**) and after (**vii**–**xii**) skin bend test. Hydrogel break points are marked with yellow arrows.

3.5. Ru/SPS Cross-Linked GelMA-Chitosan Hydrogel Precursor Solution Is Shear-Thinning, Viscous and Injectable at 37 °C

The rheological properties of Ru/SPS containing GelMA (15%, *w*/*v*), chitosan (1%, *w*/*v*), and GelMA-chitosan (GelMA 15% and chitosan 1%, *w*/*v*) precursor solutions were studied based on promising results from mechanical and adhesive test analysis. Rheological properties of GelMA, GelMA-chitosan, and chitosan solutions containing Ru/SPS at 37 °C were monitored to investigate the effect of different shear rates ranging from 0.1 to 1000 1/s on shear stress and viscosity. As shown in Figure 5A, the viscosity decreased as the shear rate increased, indicating molecular rearrangement of polymer in the flow direction. However, in the low shear rate range (≈0.1–30 1/s), the viscosity of GelMA solution decreased by nearly 1.5 orders of magnitude and remained nearly constant (≈0.03 Pa.s). At shear rates greater than 100 1/s, it demonstrated a constant value, indicating Newtonian behaviour. Chitosan (1%, *w*/*v*) solution showed shear-thinning behaviour followed by a Newtonian flow behaviour. The viscosity of GelMA-chitosan solutions was generally higher than the GelMA or Chitosan solutions alone, and decreased with the shear rate increase, indicating a shear-thinning behaviour. Similar phenomena were observed in the shear stress vs shear rate curve (Figure 5B).

The range of viscoelastic behaviour of GelMA, chitosan and GelMA-chitosan solution was quantified in amplitude sweep (Supplementary Figure S6A). The flow point of GelMA (15%, *w*/*v*) solution, where storage (G′) and loss (G″) modulus crossed several times within a very short strain range (0.1–1% strain), is shown in Supplementary Figure 6A. The G′ value of GelMA solution dominated G″ within 1–30% strain, and after that, a cross-over of G″ and G′ was observed, and G″ exhibited an independence of the applied strain. The chitosan solution represented the cross-over point at around 40% strain. On the other hand, GelMA-chitosan solution showed higher G″ values than G′ of strain sweep without any cross-over point. The values of G′ and G″ were independent within the strain range of 0.1–40% and decreased afterwards. The amplitude sweep revealed that 1% strain is far below the critical strain limits of all hydrogel precursor solutions, and this strain value was utilized a constant parameter in the frequency sweep.

Frequency sweeps in the range of 0.01–100 Hz were performed at 1% strain and 37 °C to determine the strength of the polymer network, as shown in Supplementary Figure S6B. The G′ value was higher than G″ for GelMA before and after cross-over points at around 40 and 80 Hz, respectively (Supplementary Figure S6B). Chitosan displayed higher G′ values than G″ values throughout the frequency sweep. However, chitosan (1%, *w*/*v*) added to GelMA (15%, *w*/*v*) showed higher G″ values than G′ throughout the frequency sweep (Supplementary Figure S6B).

The behaviour of polymer solutions was determined by the loss factor values where $\tan \delta > 1$ and $\tan \delta < 1$ indicate viscous and solid-like behaviour, respectively. Within a very short frequency range (1–10 Hz), GelMA solution showed relatively low values of $\tan \delta$ ($\tan \delta < 1$) till 5 Hz and higher values ($\tan \delta > 1$) afterwards (Figure 5C). Chitosan solutions exhibited solid-like behaviour within a short frequency range. However, GelMA-chitosan solutions exhibited viscous behaviour ($\tan \delta > 1$) within the short frequency range (Figure 5C). GelMA and chitosan solutions showed a decrease in complex viscosity at around 2 Hz and increased dramatically afterwards. Complex viscosity also increased with frequency in GelMA-chitosan solutions (Supplementary Figure S6C).

Temperature can affect the viscosity and modulus of a polymer solution because the molecular interactions between polymer chains are sensitive to thermal fluctuations. Therefore, it is important to maintain the temperature of the polymer solution at the optimal level to avoid any drastic changes in shear stress. To examine the influence of temperature on the modulus and viscosity of polymer solutions, we conducted a temperature ramp from 40–4 °C at 1% strain and 1 Hz frequency with a decrease rate of 1 °C/min. The values of storage/elastic (G′) and loss/viscous (G″) modulus of GelMA, chitosan and GelMA-chitosan solutions at different temperatures (40–4 °C) with a cooling rate of 1 °C/min are displayed in Figure 5D. GelMA exhibited liquid or viscous behaviour with a higher G″ than G′ at an initial temperature of 40 °C and a sharp increase in G′ than G″ were observed when temperature decreased. Additionally, a cross-over between G′ and G″ occurred upon cooling, designated the gel point, implying a transition from a solution to a gel state as the temperature decreased at around 23 °C. Viscoelastic liquid-like behaviour was observed in GelMA-chitosan solutions at a temperature around 40 °C; however, gel-like behaviour

was observed below the cross-over point at around 32 °C. On the other hand, chitosan solutions showed liquid behaviour throughout the temperature sweep (Figure 6D). Supplementary Figure S6D depicts the complex viscosity (η*) measurements, taken over a temperature range of 40 °C to 4 °C at a cooling rate of 1 °C/min. All hydrogel precursor solutions showed increased complex viscosity with decreasing temperature in the temperature sweep, with GelMA and GelMA-chitosan solutions showing comparable complex viscosity after 10 °C (Supplementary Figure S6D).

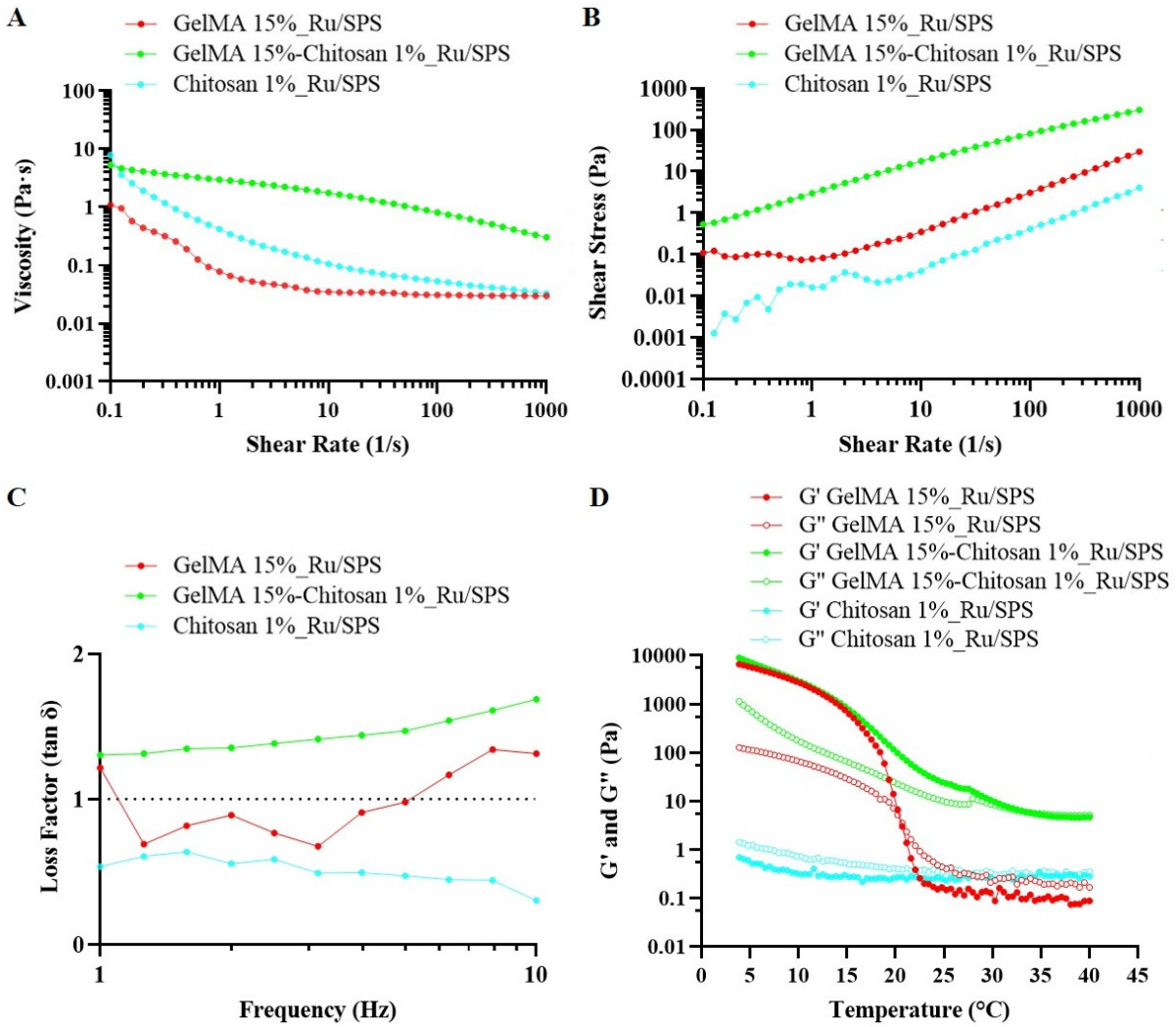

Figure 5. Rheological characterization of hydrogel polymer blends. Shear dependent viscosity (**A**), shear stress versus shear rate (**B**) loss factor (**C**) for GelMA (15%, *w/v*), GelMA (15%, *w/v*) with chitosan (1%, *w/v*) solution at 37 °C. Temperature sweep (**D**) of GelMA (15%, *w/v*), chitosan (1%, *w/v*) and GelMA-chitosan (GelMA 15% and chitosan 1%, *w/v*) solutions from 40–4 °C at 1% strain and 1 Hz frequency with a decrease rate of 1 °C/min.

4. Discussion

Bioadhesives are highly regarded for their potential to enhance wound healing by lowering surgical duration, minimizing invasiveness, and preventing body fluid leakage. Clinical applicability of bioadhesives is primarily determined by their elasticity, adhesiveness, and tensile strength [66]. This study presents the first comparative analysis of mechanical and adhesive properties of GelMA-chitosan hydrogels crosslinked using Ru/SPS, LAP, and Irgacure photo-initiators. The findings provide a foundation for creating Ru/SPS cross-linked hydrogels that are highly adhesive, mechanically robust, and injectable, with properties tuneable based on GelMA and chitosan concentration and photo-cross-linking conditions.

GelMA-chitosan hydrogels demonstrated higher CM than GelMA hydrogels (Figure 2A). Moreover, the CM of GelMA-chitosan in this study was higher than other photocured GelMA-chitosan hydrogels previously studied [67]. Furthermore, GelMA-chitosan hydrogels had lower SR than GelMA hydrogels in both Ru/SPS and LAP groups (Figure 2B). This reduction in SR may be attributed to chitosan forming an interpenetrating network (IPN) with

the covalently cross-linked GelMA, thereby limiting free space within the hydrogel structure and contributing to an increase in CM after overnight incubation in PBS (pH = 7.4). Additionally, the degree of deacetylation (DDA) could have influenced the outcome [68–70]. The high DDA of chitosan (75–85%) in this study may have facilitated higher intermolecular bonding between amino groups, resulting in enhanced crystallinity [69,71], increased CM and reduced SR, compared to GelMA hydrogels. Furthermore, higher cross-link density in GelMA-chitosan hydrogels, may have led to higher CM and lower SR compared to GelMA hydrogels [42,58]. However, the GelMA hydrogels cross-linked by Irgacure showed a greater decline in SR than the GelMA-chitosan hydrogels (Figure 2B), which could be attributed to the Irgacure concentration and cross-linking time. Irgacure is a Type I photoinitiator with weak absorbance at 365 nm (molar extinction coefficient at 365, $\varepsilon = 4\ M^{-1}\ cm^{-1}$) [72] and is more susceptible to oxygen inhibition than the Ru/SPS cross-linking system [73]. In order to address these limitations, we used Irgacure at a concentration of 0.25% (*w*/*v*) and cross-linked the hydrogel precursor solution for 15 min. This likely led to complete cross-linking of the GelMA network and reducing the SR. When chitosan was added, it may not have been able to establish hydrogen bonds with the fully cross-linked GelMA network and instead became trapped within the structure, permitting water permeation. However, further investigation is necessary to substantiate this hypothesis.

The Ru/SPS cross-linked GelMA-chitosan (GelMA 15% and chitosan 1%, *w*/*v*) hydrogel had a CM of 246 kPa [69], which approaches the CM range observed in human cartilage (0.4–0.9 MPa, unconfined compression) [74], and surpasses that of other soft tissues (10–200 kPa) [75,76], suggesting its potential for various soft tissue repair applications. In contrast to LAP [72], Ru/SPS is a type II photoinitiator with a high molar extension coefficient in the visible light range ($\varepsilon \approx 14{,}600\ M^{-1}\ cm^{-1}$ at 450 nm) that cross-linked the polymers by radical polymerization and di-tyrosine bonding [55,73]. Upon exposure to light, Ru^{2+} is oxidized to Ru^{3+} and transfers electrons to SPS and forms sulfate radicals [77], which might have initiates methacryloyl groups in GelMA [55,73]. Additionally, Ru^{3+} promotes oxidation of tyrosine residues and formation of di-tyrosine cross-links in the protein groups [78]. The diverse cross-linking mechanism likely enhanced the CM of GelMA-chitosan hydrogels cross-linked with Ru/SPS, similar to our previous research where glycol chitosan was incorporated with GelMA [53].

Semi- or interpenetrating polymer networks (IPN) are formed when hydrophilic polymer chains penetrate another cross-linked polymeric network, affecting mechanical properties. In semi-IPN, only one cross-linked network forms physically or chemically, while in IPN, two or more cross-linked networks form and interpenetrate each other [79]. Suo et al. prepared semi-IPN and IPN GelMA-chitosan hydrogels utilizing photo-cross-linking and basification [67]. Our study evaluated the effect of pH on Ru/SPS cross-linked hydrogels, as electrostatic interactions may be influence the IPN state. GelMA hydrogels exhibited lower CM than GelMA-chitosan hydrogels at pH 5–7, which became significantly lower at pH 8–9. Moreover, GelMA hydrogels had higher SR than chitosan containing hydrogels in all pH groups, except for the pH 5 group (Figure 2C,D). One possible explanation could be the isoelectric point (IEP) of GelMA, which falls within the pH range of 7–9 [80,81]. The methacrylation reaction functionalizes a portion of the amine and hydroxyl groups of gelatin, with amine groups reacting predominantly [57,82,83]. As a result, the proportion of free amine side groups decreases, and free carboxylic acid functional groups become more prevalent. When a GelMA hydrogel is allowed to swell in media with a pH higher than its IEP, the carboxyl groups are deprotonated, whereas, at a pH below the IEP, the amine groups are protonated [84]. Nonetheless, because the concentration of amine groups is lower than that of carboxylic acid groups [85], the pH above the IEP has a stronger effect [84]. When compared to neutral hydrogels, highly charged hydrogels are more hydrophilic and, as a result, swell more [86,87]. At pH levels below the IEP, the protonation of amine groups may have enhanced electrostatic repulsion, increasing water absorption and reducing CM. At pH levels above the IEP, the carboxyl groups become more deprotonated. This leads to an increase in water absorption and a decrease in CM due to the electrostatic repulsion of carboxyl groups (Figure 2C,D). In contrast to GelMA, chitosan is insoluble in water with a pH higher than 6.2 [88]. Chitosan is protonated at lower pH conditions, and due to the electrostatic repulsion of chitosan chains, chitosan gets entrapped in the other polymer network and forms a semi-IPN structure. When chitosan is exposed to a higher pH than 6.2, deprotonation leads to the formation of another network by extensive hydrophobic interactions and hydrogen bonding between adjacent chitosan chains, forming the IPN structure with GelMA [88,89]. The formation of semi-IPN or IPN can preserve each network's characteristics of the cross-linked structure and improve the stability and mechanical properties [90,91]. The precursor solution for GelMA-chitosan hydrogels had a pH of around 5.5, as determined by pH strip analysis. Consequently, when GelMA-chitosan hydrogels were incubated in various pH solutions for 2 h, they may have not fully equilibrated with the external pH conditions. As a result, semi-IPN formation in GelMA-chitosan hydrogels can be expected at pH 5–7, increasing CM and decreasing SR (Figure 2C,D). Conversely, for GelMA-chitosan hydrogels kept at pH 8 and 9, IPN structuring between these two polymers may explain the significantly increased CM and decreased SR (Figure 2C,D).

The pH is a vital parameter influenced by chemical and biochemical processes in the body and may change in different conditions and diseases. The mean value of synovial fluid (SF) pH of normal joint has been reported 7.43 (range, 7.31–7.64) [91] and 7.77 (range, 7.72–7.81) [92] while it has been reported 7.38 in osteoarthritis [91], and ≤7.5 in rheumatoid arthritis (RA) [93]. Moreover, a pH range of 6.6–7.4 was reported in various joint diseases and conditions [94,95]. These findings suggest that the pH of SF in various joint diseases and conditions typically is near-neutral, at or above pH 7, creating a favourable environment for GelMA-chitosan hydrogels to form semi-IPN or IPN structures, thereby enhancing the CM of the hydrogels. In contrast, the pH of the skin is typically acidic, ranging from 4 to 6, while the internal environment of the body maintains a neutral to slightly alkaline pH of approximately 7.4 [96,97]. Therefore, the acidic pH of the skin is anticipated to enhance the formation of a semi-IPN in this hydrogel system. Acute wounds often have a pH of 4–6, with the mild acidity preventing bacterial colonization. In contrast, chronic wounds are more alkaline (pH: 7–9), making them more susceptible to bacterial invasion and colonization [98,99]. All of these findings suggest that this hydrogel system will be able to create semi-IPN and IPN structures with damaged skin surfaces under both acute and chronic conditions. Moreover, the antibacterial property of the chitosan [100] may limit the bacterial colonization at the affected site. However, further research is necessary to validate these hypotheses.

Effectiveness of a bioadhesive is influenced by the balance between its adhesive and cohesive forces [101]. Bioadhesive failure can manifest as insufficient cohesive strength within the bioadhesive, inadequate adhesive strength at the tissue-bioadhesive interface, or complete tearing of the specimen due to the bioadhesive bond surpassing the mechanical strength of the specimen [101]. Chitosan significantly enhanced the adhesive and cohesive strength of hydrogels in tensile tests with cartilage, as indicated by higher UTS and cohesive failure, regardless of the photo-initiator (Figures 3B,F and S5). However, only the Ru/SPS cross-linked group showed a substantial increase in TSML and toughness of GelMA-chitosan hydrogels (Figures 3D and S4H). Based on the promising results of the Ru/SPS cross-linked GelMA-chitosan hydrogel, we performed shear and tensile adhesion tests utilizing caprine skin. In the tensile test, GelMA-chitosan hydrogels exhibited comparable TM to GelMA hydrogels, but significantly higher UTS, TSML and tensile toughness (Figure 4A–D). However, in the lap shear test, the GelMA and GelMA-chitosan hydrogel exhibited promising yet similar values of shear modulus (SM), ultimate shear stress (USS), shear strain at maximum load (SSML), and shear toughness (Figure 4E–H) [80]. The enhanced adhesive strength of GelMA-chitosan hydrogels can be attributed to the intermolecular and electrostatic bonding, as well as entanglement of chitosan chains inside the GelMA network, as previously observed for GelMA-glycol chitosan tested with bovine osteochondral constructs [53].

The adhesive properties of GelMA-chitosan hydrogel were tested and validated in an ex vivo joint study under simulated conditions, using LAP and Ru/SPS as visible light photo-initiators. Ru/SPS cross-linked GelMA and GelMA-chitosan hydrogels exhibited promising adhesive strength and toughness, and the application of fingertip pressure was ineffective in removing the hydrogels, suggesting a strong integration with the original cartilage (Figure 3A(v,vi)). However, while LAP cross-linked GelMA hydrogels maintained stability during the joint movement study, GelMA-chitosan hydrogels failed to effectively integrate with cartilage defects (Figure 3A(viii)). The failure of bonding can be attributed to LAP's inability to form dityrosine bonds, as well as inadequate electrostatic interactions facilitated by chitosan with the native tissue.

Bioadhesive hydrogels designed for wound healing also must exhibit both robust initial adherence and the ability to conform to the dynamic alterations of the skin surface, including flexibility and elasticity, throughout the healing process. The skin is a highly elastic and constantly moving organ that experiences stretching, compression, and shear pressures during daily activities. Moreover, during the healing process, the skin contraction will exert mechanical forces on the surrounding tissue. Under these circumstances, if the adhesive bond is not sufficiently strong, it may result in the detachment of the hydrogel, thereby hindering the healing process. The effectiveness of the Ru/SPS cross-linked GelMA-chitosan bioadhesive hydrogel was also validated through an ex vivo skin bend test conducted under simulated skin conditions. The GelMA-chitosan hydrogel showed more robust adhesion to the skin compared to the GelMA group (Figure 3B), indicating its potential for effective performance in dynamic environment (Supplementary Video S3).

In adhesive tests, Ru/SPS cross-linked GelMA-chitosan hydrogel exhibited a promising adhesive strength of approximately 100 kPa when used with osteochondral constructs (Figure 3B). This adhesive strength is significantly greater than that of other bioadhesives previously investigated for cartilage repair, such as fibrin glue (fibrin) [102–105], chondrointin sulphate based poly(ethylene glycol) diacrylate (PEGDA) hydrogels [106], tyramine-modified hyaluronic acid (HA-Tyr) hydrogels [105], and microbial transglutaminase containing photo-cross-linkable GelMA bioadhesive hydrogel [107]. Additionally, GelMA-chitosan hydrogel showed adhesive strength to native skin around 25 kPa, which is higher than that of other hydrogels studied for skin wound healing such as quaternized lignin (QL) functionalized poly(hexamethylene biguanide) hydrochloride (PHMB) complex

incorporated polyacrylamide (QL–PHMB–PAM) hydrogel (17.0 kPa) [108], and fungal-derived carboxymethyl chitosan (FCMCS) hydrogel (13.9 ± 2.8 kPa) [109]. Moreover, despite the lack of significant changes in shear properties with the incorporation of chitosan, the overall adhesive performance of both hydrogels remains robust, suggesting that the Ru/SPS cross-linking system effectively enhances adhesion. The shear strength of GelMA-chitosan hydrogel (~43 kPa) observed in this study exceeds that reported for other hydrogels evaluated in skin wound healing studies such as silk fibroin (SF) and tannic acid (TA) combined with silver nanoparticles (AgNPs) hydrogels (14.3 ± 1.9 kPa-28.8 ± 2.3 kPa) [61], commercially available fibrin glue (15.4 ± 2.8 kPa) [62], chitosan-tannic acid-silk fibrion CS4/TA2/SF1 hydrogel (29.7 ± 0.4 kPa) [63], OHA-Dop + $NaIO_4$ hydrogel (15.2 kPa) [64], CSG-PEG/DMA9/Zn hydrogel (7.2 to 11.5 kPa) [65]. Sutures and staples are the conventional techniques used to close wounds and injuries in the skin and cartilage. However, they often result in toxicity [110], inflammation [111], undesirable matrix remodeling, scar tissue formation [111], post-operative pain [112], and loss of cells in the peri-sutural area [113,114]. Additionally, they can lead to the development of cracks, the formation of suture tracks, and the need for repeated surgeries or permanent retention of suture materials [113,114]. While staples are a rapid solution in mass casualty scenarios, they are not appropriate in all circumstances. The promising results from mechanical and adhesive tests suggest that the Ru/SPS cross-linked GelMA-chitosan hydrogel has the potential to be a practical substitute for conventional sutures. Moreover, this hydrogel system is highly effective in areas where tissues experience mechanical stress or deformation, such as joints or skin, demonstrating its potential for enhancing tissue repair and regeneration in clinical settings.

Injection of the hydrogel precursor solution followed by photo-crosslinking would be a convenient clinical application method, but requires solution to be injectable. Injectable materials should have low viscosity across different injection rates for smooth and efficient delivery. The correlation between viscosity and injection pressure (IP) of submucosal injection materials (SIM) has been thoroughly investigated, revealing that both Newtonian and shear-thinning materials are viable options for SIM applications [115]. Individually, GelMA and chitosan solutions exhibited shear-thinning behaviour at low shear rates and transitioned to Newtonian behaviour at higher shear rates, suggesting structural deformation in GelMA and hydrogen bond disruption in chitosan (Figure 5A,B). In contrast, GelMA-chitosan solutions demonstrated shear-thinning properties over a broad range of shear rates, indicating the degradation of hydrogen bonding between chitosan chains in the GelMA network and their molecular orientation towards the flow direction (Figure 5A,B). Consistent with these results, the shear-thinning GelMA-chitosan hydrogel precursor solutions were effectively administered to cartilage defects through a 19-gauge needle at 37 °C, confirming the injectability of this hydrogel system. GelMA-chitosan hydrogel pre-cursor solutions exhibited liquid-like behaviour ($\tan \delta > 1$) within the low frequency range (Figure 5C), yet the frequency sweeps suggest that the viscosity is likely to increase at higher frequencies (Supplementary Figure S6C), which should be taken into account when applying the GelMA-chitosan hydrogel precursor solution. Additionally, the thermal sensitivity of GelMA-chitosan hydrogel solution should be considered during application, as it behaves more like a solid and may not be injectable at lower temperatures such as 25 °C (Figures 5D and S6D).

Chitosan is a biocompatible and biodegradable polymer. Despite promising outcomes of the GelMA-chitosan hydrogel, a limitation of this study is the absence of a cell study, which would be needed to extend the applications to tissue engineering, where cells are encapsulated in the material. In a separate study, we investigated the biodegradability of GelMA-glycol chitosan hydrogel utilizing collagenase and lysozyme [53], where complete degradation of the hydrogel confirmed the biodegradability. The current study did not include further biodegradability assessment of the GelMA-chitosan hydrogel. However, a biodegradation study is warranted for future research to investigate and adjust the hydrogel degradation rate, aligning with the tissue repair dynamics. This study provides a comprehensive evaluation of only the mechanical and adhesive properties of the GelMA-chitosan hydrogel, utilizing acid soluble chitosan. Although our previous study demonstrated promising results with water soluble glycol chitosan for osteochondral defect repair [53], this study focuses on acid soluble chitosan to produce a easy-to-use bioadhesive hydrogel due to its availability, cost-effectiveness and viscosity which may enhance the adhesive properties. The limitations underscore the need for cytocompatibility testing and in vivo studies in future to establish a robust conclusion regarding the potential of the GelMA-chitosan bioadhesive formulations for repair of damaged cartilage and skin.

5. Conclusions

Bioadhesives are increasingly recognized as a promising alternative to traditional surgical methods in tissue repair. The study highlights the enhanced mechanical and adhesive properties of Ru/SPS photo-polymerized natural polymer-based GelMA-chitosan hydrogel, which offers a simple preparation protocol and easy applicability for cartilage and skin damage repair. Additionally, this shear-thinning and injectable hydrogel holds

significant potential for diverse applications tissue repair. Future studies should investigate this bioadhesive hydrogel for various tissue engineering approaches, which could expand in vivo applications.

Supplementary Materials

The additional data and information can be downloaded at: https://media.sciltp.com/articles/others/250928094217742 8/RMD-2508000308-SI-FC.pdf.

Author Contributions

S.P., T.J.K., K.S., P.A.T., and C.M. designed the study. T.J.K., K.S., and P.A.T. supervised the project. S.P. performed all the experiments and analysed the data. A.W. and J.W.D. assisted in image processing and mould preparations. All authors participated in writing, interpreting the analysed data, and reviewing the manuscript. All authors have read and agreed to the published version of the manuscript.

Funding

The project was financially supported by an Australian Government Research Stipend Scholarship (RTP).

Institutional Review Board Statement

Not applicable.

Informed Consent Statement

Not applicable.

Data Availability Statement

The data that support the findings of this study are available from the corresponding author upon reasonable request.

Conflicts of Interest

T.J.K and C.M. are co-founders and shareholders in Gelomics, Pty Ltd.

References

1. Naahidi, S.; Jafari, M.; Logan, M.; et al. Biocompatibility of Hydrogel-Based Scaffolds for Tissue Engineering Applications. *Biotechnol. Adv.* **2017**, *35*, 530–544. https://doi.org/10.1016/J.BIOTECHADV.2017.05.006.
2. Hu, W.; Wang, Z.; Xiao, Y.; et al. Advances in Crosslinking Strategies of Biomedical Hydrogels. *Biomater. Sci*. **2019**, *7*, 843. https://doi.org/10.1039/c8bm01246f.
3. Van Vlierberghe, S.; Dubruel, P.; Schacht, E. Biopolymer-Based Hydrogels as Scaffolds for Tissue Engineering Applications: A Review. *Biomacromolecules* **2011**, *12*, 1387–1408. https://doi.org/10.1021/BM200083N.
4. Choi, B.; Kim, S.; Lin, B.; et al. Cartilaginous Extracellular Matrix-Modified Chitosan Hydrogels for Cartilage Tissue Engineering. *ACS Appl. Mater. Interfaces* **2014**, *6*, 20110–20121. https://doi.org/10.1021/AM505723K.
5. Yazdimamaghani, M.; Vashaee, D.; Assefa, S.; et al. Hybrid Macroporous Gelatin/Bioactive-Glass/Nanosilver Scaffolds with Controlled Degradation Behavior and Antimicrobial Activity for Bone Tissue Engineering. *J. Biomed. Nanotechnol.* **2014**, *10*, 911–931. https://doi.org/10.1166/JBN.2014.1783.
6. Wei, W.; Ma, Y.; Yao, X.; et al. Advanced Hydrogels for the Repair of Cartilage Defects and Regeneration. *Bioact. Mater.* **2021**, *6*, 998–1011. https://doi.org/10.1016/J.BIOACTMAT.2020.09.030.
7. Lin, H.; Yin, C.; Mo, A.; et al. Applications of Hydrogel with Special Physical Properties in Bone and Cartilage Regeneration. *Materials* **2021**, *14*, 235. https://doi.org/10.3390/MA14010235.
8. Shaikh, R.; Raj Singh, T.; Garland, M.; et al. Mucoadhesive Drug Delivery Systems. *J. Pharm. Bioallied Sci.* **2011**, *3*, 89–100. https://doi.org/10.4103/0975-7406.76478.
9. Zhang, L.; Liu, M.; Zhang, Y.; et al. Recent Progress of Highly Adhesive Hydrogels as Wound Dressings. *Biomacromolecules* **2020**, *21*, 3966–3983. https://doi.org/10.1021/ACS.BIOMAC.0C01069.
10. Zhu, J.; Marchant, R.E. Design Properties of Hydrogel Tissue-Engineering Scaffolds. *Expert. Rev. Med. Devices* **2011**, *8*, 607–626. https://doi.org/10.1586/ERD.11.27.
11. Lutolf, M.P. Biomaterials: Spotlight on Hydrogels. *Nat. Mater.* **2009**, *8*, 451–453. https://doi.org/10.1038/NMAT2458.
12. Jin, M.; Shi, J.; Zhu, W.; et al. Polysaccharide-Based Biomaterials in Tissue Engineering: A Review. *Tissue Eng. Part. B Rev.* **2021**, *27*, 604–626. https://doi.org/10.1089/TEN.TEB.2020.0208.

13. Yang, Q.; Peng, J.; Xiao, H.; et al. Polysaccharide Hydrogels: Functionalization, Construction and Served as Scaffold for Tissue Engineering. *Carbohydr. Polym.* **2022**, *278*, 118952. https://doi.org/10.1016/J.CARBPOL.2021.118952.
14. Zhu, T.; Mao, J.; Cheng, Y.; et al. Recent Progress of Polysaccharide-Based Hydrogel Interfaces for Wound Healing and Tissue Engineering. *Adv. Mater. Interfaces* **2019**, *6*, 1900761. https://doi.org/10.1002/ADMI.201900761.
15. Bao, Z.; Xian, C.; Yuan, Q.; et al. Natural Polymer-Based Hydrogels with Enhanced Mechanical Performances: Preparation, Structure, and Property. *Adv. Healthc. Mater.* **2019**, *8*, 1900670. https://doi.org/10.1002/ADHM.201900670.
16. Lih, E.; Lee, J.S.; Park, K.M.; et al. Rapidly Curable Chitosan-PEG Hydrogels as Tissue Adhesives for Hemostasis and Wound Healing. *Acta Biomater.* **2012**, *8*, 3261–3269. https://doi.org/10.1016/J.ACTBIO.2012.05.001.
17. Nie, W.; Yuan, X.; Zhao, J.; et al. Rapidly in Situ Forming Chitosan/ε-Polylysine Hydrogels for Adhesive Sealants and Hemostatic Materials. *Carbohydr. Polym.* **2013**, *96*, 342–348. https://doi.org/10.1016/J.CARBPOL.2013.04.008.
18. Ono, K.; Ishihara, M.; Ozeki, Y.; et al. Experimental Evaluation of Photocrosslinkable Chitosan as a Biologic Adhesive with Surgical Applications. *Surgery* **2001**, *130*, 844–850. https://doi.org/10.1067/MSY.2001.117197.
19. Ryu, J.H.; Hong, S.; Lee, H. Bio-Inspired Adhesive Catechol-Conjugated Chitosan for Biomedical Applications: A Mini Review. *Acta Biomater.* **2015**, *27*, 101–115. https://doi.org/10.1016/J.ACTBIO.2015.08.043.
20. Kim, I.Y.; Seo, S.J.; Moon, H.S.; et al. Chitosan and Its Derivatives for Tissue Engineering Applications. *Biotechnol. Adv.* **2008**, *26*, 1–21. https://doi.org/10.1016/J.BIOTECHADV.2007.07.009.
21. Shi, C.; Zhu, Y.; Ran, X.; et al. Therapeutic Potential of Chitosan and Its Derivatives in Regenerative Medicine. *J. Surg. Res.* **2006**, *133*, 185–192. https://doi.org/10.1016/J.JSS.2005.12.013.
22. Nawrotek, K.; Tylman, M.; Rudnicka, K.; et al. Chitosan-Based Hydrogel Implants Enriched with Calcium Ions Intended for Peripheral Nervous Tissue Regeneration. *Carbohydr. Polym.* **2016**, *136*, 764–771. https://doi.org/10.1016/J.CARBPOL.2015.09.105.
23. Elviri, L.; Bianchera, A.; Bergonzi, C.; et al. Controlled Local Drug Delivery Strategies from Chitosan Hydrogels for Wound Healing. *Expert. Opin. Drug Deliv.* **2017**, *14*, 897–908. https://doi.org/10.1080/17425247.2017.1247803.
24. Moura, M.J.; Faneca, H.; Lima, M.P.; et al. In Situ Forming Chitosan Hydrogels Prepared via Ionic/Covalent Co-Cross-Linking. *Biomacromolecules* **2011**, *12*, 3275–3284. https://doi.org/10.1021/bm200731x.
25. Jin, R.; Moreira Teixeira, L.S.; Dijkstra, P.J.; et al. Injectable Chitosan-Based Hydrogels for Cartilage Tissue Engineering. *Biomaterials* **2009**, *30*, 2544–2551. https://doi.org/10.1016/J.BIOMATERIALS.2009.01.020.
26. Tan, H.; Chu, C.R.; Payne, K.A.; et al. Injectable in Situ Forming Biodegradable Chitosan-Hyaluronic Acid Based Hydrogels for Cartilage Tissue Engineering. *Biomaterials* **2009**, *30*, 2499–2506. https://doi.org/10.1016/J.BIOMATERIALS.2008.12.080.
27. Amsden, B.G.; Sukarto, A.; Knight, D.K.; et al. Methacrylated Glycol Chitosan as a Photopolymerizable Biomaterial. *Biomacromolecules* **2007**, *8*, 3758–3766. https://doi.org/10.1021/BM700691E.
28. Lu, T.J.; Chiu, F.Y.; Chiu, H.Y.; et al. Chondrogenic Differentiation of Mesenchymal Stem Cells in Three-Dimensional Chitosan Film Culture. *Cell Transplant.* **2017**, *26*, 417. https://doi.org/10.3727/096368916X693464.
29. Lastra, M.L.; Molinuevo, M.S.; Cortizo, A.M.; et al. Fumarate Copolymer-Chitosan Cross-Linked Scaffold Directed to Osteochondrogenic Tissue Engineering. *Macromol. Biosci.* **2017**, *17*. https://doi.org/10.1002/MABI.201600219.
30. Man, Z.; Hu, X.; Liu, Z.; et al.Transplantation of Allogenic Chondrocytes with Chitosan Hydrogel-Demineralized Bone Matrix Hybrid Scaffold to Repair Rabbit Cartilage Injury. *Biomaterials* **2016**, *108*, 157–167. https://doi.org/10.1016/J.BIOMATERIALS.2016.09.002.
31. Rodrigues, M.N.; Oliveira, M.B.; Costa, R.R.; et al.Chitosan/Chondroitin Sulfate Membranes Produced by Polyelectrolyte Complexation for Cartilage Engineering. *Biomacromolecules* **2016**, *17*, 2178–2188. https://doi.org/10.1021/ACS.BIOMAC.6B00399.
32. Naderi-Meshkin, H.; Andreas, K.; Matin, M.M.; et al. Chitosan-Based Injectable Hydrogel as a Promising in Situ Forming Scaffold for Cartilage Tissue Engineering. *Cell Biol. Int.* **2014**, *38*, 72–84. https://doi.org/10.1002/CBIN.10181.
33. Feng, P.; Luo, Y.; Ke, C.; et al. Chitosan-Based Functional Materials for Skin Wound Repair: Mechanisms and Applications. *Front. Bioeng. Biotechnol.* **2021**, *9*. https://doi.org/10.3389/FBIOE.2021.650598.
34. Ogawa, K.; Yui, T.; Okuyama, K. Three D Structures of Chitosan. *Int. J. Biol. Macromol.* **2004**, *34*, 1–8. https://doi.org/10.1016/j.ijbiomac.2003.11.002.
35. Hamedi, H.; Moradi, S.; Hudson, S.M.; et al. Chitosan Based Hydrogels and Their Applications for Drug Delivery in Wound Dressings: A Review. *Carbohydr. Polym.* **2018**, *199*, 445–460. https://doi.org/10.1016/J.CARBPOL.2018.06.114.
36. Saravanan, S.; Leena, R.S.; Selvamurugan, N. Chitosan Based Biocomposite Scaffolds for Bone Tissue Engineering. *Int. J. Biol. Macromol.* **2016**, *93*, 1354–1365. https://doi.org/10.1016/J.IJBIOMAC.2016.01.112.
37. Wang, L.; Stegemann, J.P. Thermogelling Chitosan and Collagen Composite Hydrogels Initiated with Beta-Glycerophosphate for Bone Tissue Engineering. *Biomaterials* **2010**, *31*, 3976–3985. https://doi.org/10.1016/J.BIOMATERIALS.2010.01.131.
38. Huang, Y.; Onyeri, S.; Siewe, M.; et al. In Vitro Characterization of Chitosan-Gelatin Scaffolds for Tissue Engineering. *Biomaterials* **2005**, *26*, 7616–7627. https://doi.org/10.1016/J.BIOMATERIALS.2005.05.036.

39. Sun, M.; Sun, X.; Wang, Z.; et al. Synthesis and Properties of Gelatin Methacryloyl (GelMA) Hydrogels and Their Recent Applications in Load-Bearing Tissue. *Polymers* **2018**, *10*, 1290. https://doi.org/10.3390/POLYM10111290.
40. Levett, P.A.; Melchels, F.P.W.; Schrobback, K.; et al. A Biomimetic Extracellular Matrix for Cartilage Tissue Engineering Centered on Photocurable Gelatin, Hyaluronic Acid and Chondroitin Sulfate. *Acta Biomater.* **2014**, *10*, 214–223. https://doi.org/10.1016/J.ACTBIO.2013.10.005.
41. Annabi, N.; Rana, D.; Shirzaei Sani, E.; et al. Engineering a Sprayable and Elastic Hydrogel Adhesive with Antimicrobial Properties for Wound Healing. *Biomaterials* **2017**, *139*, 229–243. https://doi.org/10.1016/J.BIOMATERIALS.2017.05.011.
42. Assmann, A.; Vegh, A.; Ghasemi-Rad, M.; et al. A Highly Adhesive and Naturally Derived Sealant. *Biomaterials* **2017**, *140*, 115–127. https://doi.org/10.1016/J.BIOMATERIALS.2017.06.004.
43. Wang, H.; Zhou, L.; Liao, J.; et al. Cell-Laden Photocrosslinked GelMA-DexMA Copolymer Hydrogels with Tunable Mechanical Properties for Tissue Engineering. *J. Mater. Sci. Mater. Med.* **2014**, *25*, 2173–2183. https://doi.org/10.1007/S10856-014-5261-X.
44. Han, L.; Xu, J.; Lu, X.; et al. Biohybrid Methacrylated Gelatin/Polyacrylamide Hydrogels for Cartilage Repair. *J. Mater. Chem. B* **2017**, *5*, 731–741. https://doi.org/10.1039/C6TB02348G.
45. Nichol, J.W.; Koshy, S.T.; Bae, H.; et al. Cell-Laden Microengineered Gelatin Methacrylate Hydrogels. *Biomaterials* **2010**, *31*, 5536–5544. https://doi.org/10.1016/J.BIOMATERIALS.2010.03.064.
46. Schuurman, W.; Levett, P.A.; Pot, M.W.; et al. Gelatin-Methacrylamide Hydrogels as Potential Biomaterials for Fabrication of Tissue-Engineered Cartilage Constructs. *Macromol. Biosci.* **2013**, *13*, 551–561. https://doi.org/10.1002/MABI.201200471.
47. Chen, Y.C.; Lin, R.Z.; Qi, H.; et al. Functional Human Vascular Network Generated in Photocrosslinkable Gelatin Methacrylate Hydrogels. *Adv. Funct. Mater.* **2012**, *22*, 2027–2039. https://doi.org/10.1002/ADFM.201101662.
48. O'Connell, C.D.; Zhang, B.; Onofrillo, C.; et al. Tailoring the Mechanical Properties of Gelatin Methacryloyl Hydrogels through Manipulation of the Photocrosslinking Conditions. *Soft Matter* **2018**, *14*, 2142–2151. https://doi.org/10.1039/C7SM02187A.
49. Kim, C.; Young, J.L.; Holle, A.W.; et al. Stem Cell Mechanosensation on Gelatin Methacryloyl (GelMA) Stiffness Gradient Hydrogels. *Ann. Biomed. Eng.* **2020**, *48*, 893–902. https://doi.org/10.1007/S10439-019-02428-5.
50. Nguyen, K.T.; West, J.L. Photopolymerizable Hydrogels for Tissue Engineering Applications. *Biomaterials* **2002**, *23*, 4307–4314. https://doi.org/10.1016/S0142-9612(02)00175-8.
51. Lee, C.; O'Connell, C.D.; Onofrillo, C.; et al. Human Articular Cartilage Repair: Sources and Detection of Cytotoxicity and Genotoxicity in Photo-Crosslinkable Hydrogel Bioscaffolds. *Stem Cells Transl. Med.* **2020**, *9*, 302–315.
52. Zheng, Z.; Eglin, D.; Alini, M.; et al. Visible Light-Induced 3D Bioprinting Technologies and Corresponding Bioink Materials for Tissue Engineering: A Review. *Engineering* **2021**, *7*, 966–978.
53. Paul, S.; Schrobback, K.; Tran, P.A.; et al. Photo-Cross-Linkable, Injectable, and Highly Adhesive GelMA-Glycol Chitosan Hydrogels for Cartilage Repair. *Adv. Healthc. Mater.* **2023**, *12*, 2302078. https://doi.org/10.1002/ADHM.202302078.
54. Paul, S.; Schrobback, K.; Tran, P.A.; et al. GelMA-Glycol Chitosan Hydrogels for Cartilage Regeneration: The Role of Uniaxial Mechanical Stimulation in Enhancing Mechanical, Adhesive, and Biochemical Properties. *APL Bioeng.* **2023**, *7*, 036114. https://doi.org/10.1063/5.0160472.
55. Lim, K.S.; Klotz, B.J.; Lindberg, G.C.J.; et al. Visible Light Cross-Linking of Gelatin Hydrogels Offers an Enhanced Cell Microenvironment with Improved Light Penetration Depth. *Macromol. Biosci.* **2019**, *19*, 1900098. https://doi.org/10.1002/MABI.201900098.
56. Loessner, D.; Meinert, C.; Kaemmerer, E.; et al. Functionalization, Preparation and Use of Cell-Laden Gelatin Methacryloyl–Based Hydrogels as Modular Tissue Culture Platforms. *Nat. Protoc.* **2016**, *11*, 727–746. https://doi.org/10.1038/nprot.2016.037.
57. *ASTM F2458-05*; Standard Test Method for Wound Closure Strength of Tissue Adhesives and Sealants. ASTM: West Conshohocken, PA, USA, 2015. Available online: https://www.astm.org/f2458-05r15.html (accessed on 12 August 2024).
58. *ASTM F2255-24*; Standard Test Method for Strength Properties of Tissue Adhesives in Lap-Shear by Tension Loading. ASTM: West Conshohocken, PA, USA, 2024. Available online: https://www.astm.org/f2255-05r15.html (accessed on 12 August 2024).
59. Gupta, A.; Bhat, S.; Jagdale, P.R.; et al. Evaluation of Three-Dimensional Chitosan-Agarose-Gelatin Cryogel Scaffold for the Repair of Subchondral Cartilage Defects: An in Vivo Study in a Rabbit Model. *Tissue Eng. Part. A* **2014**, *20*, 3101–3111. https://doi.org/10.1089/TEN.TEA.2013.0702.
60. Mizrahi, B.; Weldon, C.; Kohane, D.S. Tissue Adhesives as Active Implants. *Stud. Mechanobiol. Tissue Eng. Biomater.* **2010**, *8*, 39–56. https://doi.org/10.1007/8415_2010_48.
61. Ke, X.; Dong, Z.; Tang, S.; et al. A Natural Polymer Based Bioadhesive with Self-Healing Behavior and Improved Antibacterial Properties. *Biomater. Sci.* **2020**, *8*, 4346–4357. https://doi.org/10.1039/D0BM00624F.
62. Mehdizadeh, M.; Weng, H.; Gyawali, D.; et al. Injectable Citrate-Based Mussel-Inspired Tissue Bioadhesives with High Wet Strength for Sutureless Wound Closure. *Biomaterials* **2012**, *33*, 7972–7983. https://doi.org/10.1016/J.BIOMATERIALS.2012.07.055.

63. Qiao, Z.; Lv, X.; He, Set al. A Mussel-Inspired Supramolecular Hydrogel with Robust Tissue Anchor for Rapid Hemostasis of Arterial and Visceral Bleedings. *Bioact. Mater.* **2021**, *6*, 2829–2840. https://doi.org/10.1016/J.BIOACTMAT.2021.01.039.
64. Yang, B.; Song, J.; Jiang, Y.; et al. Injectable Adhesive Self-Healing Multicross-Linked Double-Network Hydrogel Facilitates Full-Thickness Skin Wound Healing. *ACS Appl. Mater. Interfaces* **2020**, *12*, 57782–57797. https://doi.org/10.1021/ACSAMI.0C18948.
65. Yang, Y.; Liang, Y.; Chen, J.; et al. Mussel-Inspired Adhesive Antioxidant Antibacterial Hemostatic Composite Hydrogel Wound Dressing via Photo-Polymerization for Infected Skin Wound Healing. *Bioact. Mater.* **2021**, *8*, 341–354. https://doi.org/10.1016/J.BIOACTMAT.2021.06.014.
66. Kull, S.; Martinelli, I.; Briganti, E.; et al. Glubran2 Surgical Glue: In Vitro Evaluation of Adhesive and Mechanical Properties. *J. Surg. Res.* **2009**, *157*, e15–e21. https://doi.org/10.1016/J.JSS.2009.01.034.
67. Suo, H.; Zhang, D.; Yin, J.; et al. Interpenetrating Polymer Network Hydrogels Composed of Chitosan and Photocrosslinkable Gelatin with Enhanced Mechanical Properties for Tissue Engineering. *Mater. Sci. Eng. C* **2018**, *92*, 612–620. https://doi.org/10.1016/J.MSEC.2018.07.016.
68. Galed, G.; Miralles, B.; Paños, I.; et al. N-Deacetylation and Depolymerization Reactions of Chitin/Chitosan: Influence of the Source of Chitin. *Carbohydr. Polym.* **2005**, *62*, 316–320. https://doi.org/10.1016/J.CARBPOL.2005.03.019.
69. Cao, W.; Jing, D.; Li, J.; et al. Effects of the Degree of Deacetylation on the Physicochemical Properties and Schwann Cell Affinity of Chitosan Films. *J. Biomater. Appl.* **2005**, *20*, 157–177. https://doi.org/10.1177/0885328205049897.
70. Foster, L.J.R.; Ho, S.; Hook, J.; et al. Chitosan as a Biomaterial: Influence of Degree of Deacetylation on Its Physiochemical, Material and Biological Properties. *PLoS ONE* **2015**, *10*, e0135153. https://doi.org/10.1371/JOURNAL.PONE.0135153.
71. Ren, D.; Yi, H.; Wang, W.; et al. The Enzymatic Degradation and Swelling Properties of Chitosan Matrices with Different Degrees of N-Acetylation. *Carbohydr. Res.* **2005**, *340*, 2403–2410. https://doi.org/10.1016/J.CARRES.2005.07.022.
72. Fairbanks, B.D.; Schwartz, M.P.; Bowman, C.N.; et al. Photoinitiated Polymerization of PEG-Diacrylate with Lithium Phenyl-2,4,6-Trimethylbenzoylphosphinate: Polymerization Rate and Cytocompatibility. *Biomaterials* **2009**, *30*, 6702–6707. https://doi.org/10.1016/J.BIOMATERIALS.2009.08.055.
73. Lim, K.S.; Schon, B.S.; Mekhileri, N.V.; et al. New Visible-Light Photoinitiating System for Improved Print Fidelity in Gelatin-Based Bioinks. *ACS Biomater. Sci. Eng.* **2016**, *2*, 1752–1762. https://doi.org/10.1021/ACSBIOMATERIALS.6B00149.
74. Mow, V.C.; Guo, X.E. Mechano-Electrochemical Properties of Articular Cartilage: Their Inhomogeneities and Anisotropies. *Annu. Rev. Biomed. Eng.* **2002**, *4*, 175–209. https://doi.org/10.1146/ANNUREV.BIOENG.4.110701.120309.
75. Li, C.; Guan, G.; Reif, R.; et al. Determining Elastic Properties of Skin by Measuring Surface Waves from an Impulse Mechanical Stimulus Using Phase-Sensitive Optical Coherence Tomography. *J. R. Soc. Interface* **2012**, *9*, 831–841. https://doi.org/10.1098/RSIF.2011.0583.
76. Yang, C.; Xu, L.; Zhou, Y.; et al. A Green Fabrication Approach of Gelatin/CM-Chitosan Hybrid Hydrogel for Wound Healing. *Carbohydr. Polym.* **2010**, *4*, 1297–1305. https://doi.org/10.1016/J.CARBPOL.2010.07.013.
77. Fancy, D.A.; Denison, C.; Kim, K.; et al. Scope, Limitations and Mechanistic Aspects of the Photo-Induced Cross-Linking of Proteins by Water-Soluble Metal Complexes. *Chem. Biol.* **2000**, *7*, 697–708. https://doi.org/10.1016/S1074-5521(00)00020-X.
78. Elvin, C.M.; Vuocolo, T.; Brownlee, A.G.; et al. A Highly Elastic Tissue Sealant Based on Photopolymerised Gelatin. *Biomaterials* **2010**, *31*, 8323–8331. https://doi.org/10.1016/J.BIOMATERIALS.2010.07.032.
79. Cui, L.; Jia, J.; Guo, Y.; et al. Preparation and Characterization of IPN Hydrogels Composed of Chitosan and Gelatin Cross-Linked by Genipin. *Carbohydr. Polym.* **2014**, *99*, 31–38. https://doi.org/10.1016/J.CARBPOL.2013.08.048.
80. Eysturskard, J.; Haug, I.J.; Ulset, A.S.; et al. Mechanical Properties of Mammalian and Fish Gelatins Based on Their Weight Average Molecular Weight and Molecular Weight Distribution. *Food Hydrocoll.* **2009**, *23*, 2315–2321. https://doi.org/10.1016/J.FOODHYD.2009.06.007.
81. Lee, B.H.; Lum, N.; Seow, L.Y.; et al. Synthesis and Characterization of Types A and B Gelatin Methacryloyl for Bioink Applications. *Materials* **2016**, *9*, 797. https://doi.org/10.3390/MA9100797.
82. Shirahama, H.; Lee, B.H.; Tan, L.P.; et al. Precise Tuning of Facile One-Pot Gelatin Methacryloyl (GelMA) Synthesis. *Sci. Rep.* **2016**, *6*, 31036. https://doi.org/10.1038/srep31036.
83. Liang, J.; Grijpma, D.W.; Poot, A.A. Tough and Biocompatible Hybrid Networks Prepared from Methacrylated Poly(Trimethylene Carbonate) (PTMC) and Methacrylated Gelatin. *Eur. Polym. J.* **2020**, *123*, 109420. https://doi.org/10.1016/J.EURPOLYMJ.2019.109420.
84. Vigata, M.; Meinert, C.; Bock, N.; et al. Deciphering the Molecular Mechanism of Water Interaction with Gelatin Methacryloyl Hydrogels: Role of Ionic Strength, Ph, Drug Loading and Hydrogel Network Characteristics. *Biomedicines* **2021**, *9*, 574. https://doi.org/10.3390/BIOMEDICINES9050574/S1.
85. Yue, K.; Li, X.; Schrobback, K.; et al. Structural Analysis of Photocrosslinkable Methacryloyl-Modified Protein Derivatives. *Biomaterials* **2017**, *139*, 163–171. https://doi.org/10.1016/J.BIOMATERIALS.2017.04.050.

86. Hollingshead, S.; Liu, J.C. PH-Sensitive Mechanical Properties of Elastin-Based Hydrogels. *Macromol. Biosci.* **2020**, *20*, 1900369. https://doi.org/10.1002/MABI.201900369.
87. Percot, A.; Lafleur, M.; Zhu, X.X. New Hydrogels Based on N-Isopropylacrylamide Copolymers Crosslinked with Polylysine: Membrane Immobilization Systems. *Polymer* **2000**, *41*, 7231–7239. https://doi.org/10.1016/S0032-3861(00)00074-4.
88. Tang, Y.F.; Du, Y.M.; Hu, X.W.; et al. Rheological Characterisation of a Novel Thermosensitive Chitosan/Poly(Vinyl Alcohol) Blend Hydrogel. *Carbohydr. Polym.* **2007**, *67*, 491–499. https://doi.org/10.1016/J.CARBPOL.2006.06.015.
89. Zhu, F.; Yu, H.; Lei, W.; et al. Tough Polyion Complex Hydrogel Films of Natural Polysaccharides. *Chin. J. Polym. Sci.* **2017**, *35*, 1276–1285. https://doi.org/10.1007/S10118-017-1977-7/METRICS.
90. Rungrod, A.; Kapanya, A.; Punyodom, W.; et al. Synthesis and Characterization of Semi-IPN Hydrogels Composed of Sodium 2-Acrylamido-2-Methylpropanesulfonate and Poly(ε-Caprolactone) Diol for Controlled Drug Delivery. *Eur. Polym. J.* **2022**, *164*, 110978. https://doi.org/10.1016/J.EURPOLYMJ.2021.110978.
91. Wong, E. Clinical Laboratory Diagnostics: Use and Assessment of Clinical Laboratory Results. Lothar Thomas. Frankfurt/Main, Germany: TH-Books Verlagsgeselschaft, 1998, 1727 Pp., $149.00. ISBN 3-9805215-4-0. *Clin. Chem.* **1999**, *45*, 586–587. https://doi.org/10.1093/CLINCHEM/45.4.586A.
92. Jebens, E.H.; Monk-Jones, M.E. On the Viscosity and PH of Synovial Fluid and the PH of Blood. *J. Bone Jt. Surg. Br.* **1959**, *41*, 388–400. https://doi.org/10.1302/0301-620X.41B2.388.
93. Pfister, S.A.; Hauke, G.; Peter, H.H. Synoviaanalyse: Vorgehen in Der Praxis. *Aktuelle Rheumatol.* **1989**, *14*, 51–57. https://doi.org/10.1055/S-2008-1047470/BIB.
94. Treuhaft, P.S.; McCarty, D.J. Synovial Fluid PH, Lactate, Oxygen and Carbon Dioxide Partial Pressure in Various Joint Diseases. *Arthritis Rheum.* **1971**, *14*, 475–484. https://doi.org/10.1002/ART.1780140407.
95. Lund-Olesen, K. Oxygen Tension in Synovial Fluids. *Arthritis Rheum.* **1970**, *13*, 769–776. https://doi.org/10.1002/ART.1780130606.
96. Zlotogorski, A. Distribution of Skin Surface PH on the Forehead and Cheek of Adults. *Arch. Dermatol. Res.* **1987**, *279*, 398–401. https://doi.org/10.1007/BF00412626.
97. Raphael, K.L.; Murphy, R.A.; Shlipak, M.G.; et al. Bicarbonate Concentration, Acid-Base Status, and Mortality in the Health, Aging, and Body Composition Study. *Clin. J. Am. Soc. Nephrol.* **2016**, *11*, 308–316. https://doi.org/10.2215/CJN.06200615.
98. McLister, A.; McHugh, J.; Cundell, J.; et al. New Developments in Smart Bandage Technologies for Wound Diagnostics. *Adv. Mater.* **2016**, *28*, 5732–5737. https://doi.org/10.1002/ADMA.201504829.
99. Qin, M.; Guo, H.; Dai, Z.; et al. Advances in Flexible and Wearable PH Sensors for Wound Healing Monitoring. *J. Semicond.* **2019**, *40*, 111607. https://doi.org/10.1088/1674-4926/40/11/111607.
100. No, H.K.; Young Park, N.; Ho Lee, S.; et al. Antibacterial Activity of Chitosans and Chitosan Oligomers with Different Molecular Weights. *Int. J. Food Microbiol.* **2002**, *74*, 65–72. https://doi.org/10.1016/S0168-1605(01)00717-6.
101. Zhu, W.; Chuah, Y.J.; Wang, D.A. Bioadhesives for Internal Medical Applications: A Review. *Acta Biomater.* **2018**, *74*, 1–16. https://doi.org/10.1016/J.ACTBIO.2018.04.034.
102. Shah, N.V.; Meislin, R. Current State and Use of Biological Adhesives in Orthopedic Surgery. *Orthopedics* **2013**, *36*, 945–956. https://doi.org/10.3928/01477447-20131120-09.
103. Mehdizadeh, M.; Yang, J. Design Strategies and Applications of Tissue Bioadhesives. *Macromol. Biosci.* **2013**, *13*, 271–288. https://doi.org/10.1002/MABI.201200332.
104. Chivers, R.A.; Wolowacz, R.G. The Strength of Adhesive-Bonded Tissue Joints. *Int. J. Adhes. Adhes.* **1997**, *17*, 127–132. https://doi.org/10.1016/S0143-7496(96)00041-3.
105. Behrendt, P.; Ladner, Y.; Stoddart, M.J.; et al. Articular Joint-Simulating Mechanical Load Activates Endogenous TGF-β in a Highly Cellularized Bioadhesive Hydrogel for Cartilage Repair. *Am. J. Sports Med.* **2020**, *48*, 210–221. https://doi.org/10.1177/0363546519887909.
106. Wang, D.A.; Varghese, S.; Sharma, B.; et al. Multifunctional Chondroitin Sulphate for Cartilage Tissue-Biomaterial Integration. *Nat. Mater.* **2007**, *6*, 385–392. https://doi.org/10.1038/NMAT1890.
107. Trengove, A.; Duchi, S.; Onofrillo, C.; et al. Microbial Transglutaminase Improves Ex Vivo Adhesion of Gelatin Methacryloyl Hydrogels to Human Cartilage. *Front. Med. Technol.* **2021**, *3*. https://doi.org/10.3389/FMEDT.2021.773673.
108. Dong, Y.; Li, Y.; Fan, B.; et al. Long-Term Antibacterial, Antioxidative, and Bioadhesive Hydrogel Wound Dressing for Infected Wound Healing Applications. *Biomater. Sci.* **2023**, *11*, 2080–2090. https://doi.org/10.1039/D2BM01981G.
109. Rao, K.M.; Uthappa, U.T.; Kim, H.J.; et al. Tissue Adhesive, Biocompatible, Antioxidant, and Antibacterial Hydrogels Based on Tannic Acid and Fungal-Derived Carboxymethyl Chitosan for Wound-Dressing Applications. *Gels* **2023**, *9*, 354. https://doi.org/10.3390/GELS9050354.
110. Tummalapalli, M.; Anjum, S.; Kumari, S.; et al. Antimicrobial Surgical Sutures: Recent Developments and Strategies. *Polym. Rev.* **2016**, *56*, 607–630. https://doi.org/10.1080/15583724.2015.1119163.

111. Lock, A.M.; Gao, R.; Naot, D.; et al. Induction of Immune Gene Expression and Inflammatory Mediator Release by Commonly Used Surgical Suture Materials: An Experimental in Vitro Study. *Patient Saf. Surg.* **2017**, *11*, 16. https://doi.org/10.1186/S13037-017-0132-2.
112. Topart, P.; Vandenbroucke, F.; Lozac'h, P. Tisseel vs. Tack Staples as Mesh Fixation in Totally Extraperitoneal Laparoscopic Repair of Groin Hernias: A Retrospective Analysis. *Surg. Endosc. Other Interv. Tech.* **2005**, *19*, 724–727. https://doi.org/10.1007/S00464-004-8812-2/TABLES/3.
113. Hunziker, E.B. Articular Cartilage Repair: Basic Science and Clinical Progress. A Review of the Current Status and Prospects. *Osteoarthr. Cartil.* **2002**, *10*, 432–463. https://doi.org/10.1053/joca.2002.0801.
114. Hunziker, E.B.; Stähli, A. Surgical Suturing of Articular Cartilage Induces Osteoarthritis-Like Changes. *Osteoarthr. Cartil.* **2008**, *16*, 1067. https://doi.org/10.1016/J.JOCA.2008.01.009.
115. Yoshida, T.; Hirose, R.; Naito, Y.; et al. Viscosity: An Important Factor in Predicting the Performance of Submucosal Injection Materials. *Mater. Des.* **2020**, *195*, 109008. https://doi.org/10.1016/J.MATDES.2020.109008.